VERTIGO (VERtical Transport In the Global Ocean): a study of particle sources and flux attenuation in the North Pacific

Buesseler, K.O.[1], Trull, T.W.[2], Steinberg, D.K.[3], Silver, M.W.[4], Siegel, D.A.[5], Saitoh, S.-I.[6], Lamborg, C.H.[1], Lam, P.J.[1], Karl, D.M.[7], Jiao, N.Z.[8], Honda, M.C.[9], Elskens, M.[10], Dehairs, F.[10], Brown, S.L.[7], Boyd, P.W.[11], Bishop, J.K.B.[12], Bidigare, R.R[7]

1. Department of Marine Chemistry and Geochemistry, Woods Hole Oceanographic Institution, Woods Hole, MA 02543, USA
2. Antarctic Climate and Ecosystems Cooperative Research Centre, University of Tasmania – CSIRO Marine and Atmospheric Research, Hobart, 7001, Australia
3. Virginia Institute of Marine Science, College of William and Mary, Gloucester Point, VA 23062, USA
4. Ocean Sciences Department, University of California, Santa Cruz, CA 95064 USA
5. Institute for Computational Earth System Science, University of California, Santa Barbara, CA 93106, USA
6. Laboratory of Marine Bioresources and Environment Sensing, Graduate School of Fisheries Sciences, Hokkaido University, 3-1-1, Minato-cho, Hakodate, Hokkaido 041-8611, Japan
7. School of Ocean and Earth Sciences and Technology, University of Hawaii, Honolulu, HI 96822, USA
8. State Key Laboratory for Environmental Sciences, Xiamen University, 361005, P. R. China
9. Japan Agency for Marine-Earth Science and Technology (JAMSTEC), Mutsu Institute for Oceanography, Yokosuka, Kanagawa, 237-0061 Japan
10. Analytical and Environmental Chemistry, Free University of Brussels, Brussels, Belgium
11. NIWA Centre for Physical and Chemical Oceanography, Department of Chemistry, University of Otago, Dunedin, New Zealand
12. Lawrence Berkeley National Laboratory; University of California Berkeley, Department of Earth and Planetary Science, Berkeley, CA

ABSTRACT

The VERtical Transport In the Global Ocean (VERTIGO) study examined particle sources and fluxes through the ocean's "twilight zone" (defined here as depths below the euphotic zone to 1000 m). Interdisciplinary process studies were conducted at contrasting sites off Hawaii (ALOHA) and in the NW Pacific (K2) during 3 week occupations in 2004 and 2005, respectively. We examine in this overview paper the contrasting physical, chemical and biological settings and how these conditions impact the source characteristics of the sinking material and the transport efficiency through the twilight zone. A major finding in VERTIGO is the considerably lower transfer efficiency (T_{eff}) of particulate organic carbon (POC), POC flux 500 / 150 m, at ALOHA (20%) vs. K2 (50%). This efficiency is higher in the diatom-dominated setting at K2 where silica-rich particles dominate the flux at the end of a diatom bloom, and where zooplankton and their pellets are larger. At K2, the drawdown of macronutrients is used to assess export and suggests that shallow remineralization above our 150 m trap is significant, especially for N relative to Si. We explore here also surface export ratios (POC flux/primary production) and possible reasons why this ratio is higher at K2, especially during the first trap deployment. When we compare the 500 m fluxes to deep moored traps, both sites lose about half of the sinking POC by >4000 m, but this comparison is limited in that fluxes at depth may have both a local and distant component. Certainly, the greatest difference in particle flux attenuation is in the mesopelagic, and we highlight other VERTIGO papers that provide a more detailed examination of the particle sources, flux and processes that attenuate the flux of sinking particles. Ultimately, we contend that at least three types of processes need to be considered: heterotrophic degradation of sinking particles, zooplankton migration and surface feeding, and lateral sources of suspended and sinking materials. We have evidence that all of these processes impacted the net attenuation of particle flux vs. depth measured in VERTIGO and would therefore need to be considered and quantified in order to understand the magnitude and efficiency of the ocean's biological pump.

1. INTRODUCTION

VERtical Transport In the Global Ocean (VERTIGO) was a multidisciplinary study that set out to address the basic question: What controls the magnitude and efficiency of particle transport between the surface and deep-ocean? This transport occurs mostly through the gravitational settling of particles produced by the ocean's "biological pump" (Volk and Hoffert, 1985). This pump starts with the production of biogenic materials in the surface oceans where carbon dioxide is fixed during photosynthesis by phytoplankton in the euphotic layer. A fraction of this biogenic material is then transferred below the euphotic zone via three major processes: i) passive sinking of particulate organic matter (POM), ii) physical mixing of suspended particulates and dissolved organic matter (DOM), and iii) active transport by zooplankton vertical migration. The sinking POM includes senescent phytoplankton, zooplankton fecal pellets, molts, mucous feeding webs (e.g. larvacean houses), and aggregates of these materials, thus POM contains particulate organic carbon (POC) and all associated elements. Some POM may even become positively buoyant following partial degradation (Yayanos *et al.*, 1978).

In general, sinking particles are fragmented into smaller, non-sinking particles, chemically degraded, and consumed and respired by bacteria, zooplankton and nekton. The summation of these processes leads to flux attenuation with depth, which is referred to here as "particle remineralization". Planktonic food webs impact the attenuation of particle flux because they are the source of most sinking POM in the open ocean. Food web structure thus influences particle size, shape, density, and the content of biogenic minerals which affect sinking and remineralization rates (e.g. Fowler and Knauer, 1986). Remineralization returns POM and associated elements to dissolved inorganic forms, suspended POM and dissolved organic matter (DOM). This attenuation in particle flux vs. depth is greatest in the "twilight zone" (depths below the euphotic zone to 1000 m), and has been suggested to vary for different elements or source

particle types and as a consequence of mesopelagic food webs.

One motivation for understanding processes in the "twilight zone" is to better quantify the magnitude of the ocean carbon sink and controls on C sequestration into the deep-ocean. Particles must sink below the deepest mixed layer (typically during winter) in order to have a net impact on the atmospheric C cycle and hence climate. Thus physical controls on the depth of the euphotic zone and surface mixed layer plus the extent of upper ocean ventilation can affect the export of particulate carbon (Antia *et al.*, 2001). The extent of POC and particulate inorganic carbon (PIC) partitioning on sinking particles with depth is also critical for understanding ocean C uptake, since photosynthesis and the production of POC decreases surface ocean pCO_2, while production of calcium carbonate (calcite and aragonite), which are the main forms of PIC, would ultimately increase pCO_2 (Holligan *et al.*, 1993; Antia *et al.*, 1999; Francois *et al.*, 2002; Berelson *et al.*, 2007).

Changes in the strength of the biological pump are not necessarily sufficient to alter ocean C sequestration if upwelling of dissolved inorganic carbon and nutrients at Redfield ratio proportions is balanced by export at equivalent ratios (Michaels *et al.*, 2001). However changes in the relative remineralization length scales for C, N and P fluxes must be considered and would change this balance. In addition, changes in the magnitude of particle flux in the ocean are large, as evidenced by considerable seasonal and interannual variability in particle export and the composition of materials caught in deep-ocean moored time-series traps (Deuser, 1986; Wefer and Fischer, 1991; Honjo and Manganini, 1993; Conte *et al.*, 2001). Thus the flux of C through the twilight zone is a large and variable component of the global carbon cycle that is not necessarily in steady state, at least with respect to time-scales of deep-ocean mixing. As such, changes in export flux from the euphotic zone and subsequent transfer through the mesopelagic "twilight zone" can be expected to have important consequences for regulating net ocean C

sequestration (Buesseler *et al.*, 2007b).

Our approach in VERTIGO was to characterize the building blocks of marine particles in the surface ocean, and study changes in relative composition and flux with depth of carbon and associated elements. Our two initial hypotheses were that: 1) particle source characteristics determine transport efficiency of sinking particles, and/or 2) mid-water processes in the twilight zone determine transport efficiency. These rather general hypotheses are not new, but they frame the basic questions of study if one rejects the hypothesis that flux vs. depth patterns are constant throughout the world ocean. Also, our two VERTIGO hypotheses are not mutually exclusive and may work in tandem to produce interesting feedback mechanisms. For example, mid-water zooplankton may not be generalist particle grazers, but have specific adaptations to feed on slow or fast sinking particles, or particles with a particular elemental composition. Changes in source characteristics may thus trigger changes in remineralization or "repackaging" (reprocessing of particles) by mid-water communities. Carbon budgets over the upper 1000 m of the water column in the NE subarctic Pacific suggest that both heterotrophic bacteria and large migratory zooplankton are responsible for particle transformations in the twilight zone (Boyd *et al.*, 1999) and our own results support this combined microbial and zooplankton role in particle transport and attenuation (Steinberg *et al.*, 2007). These remineralization processes produce non-sinking (suspended) particles, and as there are considerable interactions among suspended and sinking particles in the ocean, we also sampled suspended particles in VERTIGO. Finally, even though our attention in VERTIGO was focused on the upper 500-1000 m we compared our results with traditional deep trap fluxes (>2800-4800 m) collected with time-series moorings.

The first VERTIGO flux results and a brief description of the program have recently appeared (Buesseler *et al.*, 2007b), though the full range of geochemical, biological and physical studies, as well as the novel techniques used to understand particle flux and processes that attenuate flux,

have not been described until this Special Issue of *DSRII*. This overview paper provides more details about the two study sites including macronutrient budgets and phytoplankton community structure. We also discuss here the connections between surface production, mesopelagic processes and deep ocean flux. Where appropriate, pointers to other VERTIGO manuscripts in this issue and elsewhere are made.

2. METHODS

Methods details unique to VERTIGO are provided in primary manuscripts in this Special Issue. Briefly, two types of mesopelagic sediment traps were deployed for the primary flux measurements: 1) a newly designed neutrally buoyant sediment trap (NBST), which is a free vehicle that sinks to a preprogrammed sampling depth for 3-5 day deployments and drifts with local currents, thus minimizing possible hydrodynamic biases; and 2) the "Clap-trap", a surface-tethered trap containing 8 collection tubes that are similar to the commonly used "MultiPITS" tubes (e.g. Karl *et al*., 1996), but which have been modified to clap shut at depth prior to recovery. Other traps were deployed for specific purposes, including a surface-tethered indented-rotating-sphere trap to determine *in-situ* particle sinking rates (Trull *et al.*, this volume), an "optical trap" that photographed particles settling on to a plate with hourly resolution to examine diel cycles (Bishop *et al*., in preparation), a trap equipped with an oxygen sensor to examine *in-situ* remineralization rates (Boyd *et al.*, in preparation), and traps filled with polyacrylamide gels to obtain intact aggregates (Trull *et al*, in preparation). This overview focuses on the NBST data. Detailed comparisons of the NBST and Clap-trap fluxes along with protocols for blanks, swimmer removal, sample preservation and sampling handling and analytical methods are presented in Lamborg *et al.* (this volume-a). Deep traps fluxes discussed here are from time-series moorings operated as part of ongoing sediment trap programs at ALOHA (Sharek *et al.*, 1999) and K2 (Honda *et al*., 2002).

Each cruise was organized around two trap deployments (D1 and D2) of 3, 4, 5 day duration with multiple traps at 150, 300 and 500, respectively. During each cruise, we concentrated measurements of water column properties, biological rates and community structure at 8 CTD/Rosette "biocasts" roughly every other day during a two week period. These biocasts were sampled at predawn and in close proximity to the 150 m Clap traps, and thus central to the study area and expected particle source region. Standard parameters analyzed on these biocasts and selected other stations were derived from CTD sensors (temperature, salinity, oxygen, fluorescence, light transmission and scattering) and bottle derived measurements, including on a regular basis dissolved nutrients (on frozen samples), salinity (smaller subset for sensor calibration), HPLC pigments (2 L filtration and LN_2 storage), microscopic phytoplankton ID (at sea and on preserved samples), thorium-234, particulate and dissolved C/N isotopes, bacteria counts and productivity, ^{14}C, ^{13}C and ^{15}N incubations for phytoplankton uptake, and particulate Ba and other trace metals. Open access to primary VERTIGO data sets presented here and as used in other VERTIGO manuscripts can be found at the Ocean Carbon & Biogeochemistry Data Management web site (http://ocb.whoi.edu/vertigo.html). A larger scale CTD survey of each site (survey with scales of ~100 - 200 km per side) with fewer bottle measured parameters was conducted before, in between and after the two trap deployments. At K2, we also present seasonal nutrient data from a moored remote automated sampler deployed at ~35 m (Honda and Watanabe, 2007). Particles were also collected using a Multiple Unit Large Volume Filtration System, as described previously by Bishop *et al.* (1985).

3. RESULTS AND DISCUSSION

3.1. Study Sites: general comparison of annual cycles at ALOHA and K2

We chose two field sites in the North Pacific where we expected to find large differences in the composition of sinking and suspended particles, the magnitude of particle flux, and remineralization length scales (Figure 1). These are station ALOHA, site of the Hawaii Ocean Time-series program (HOT; 22.75°N; 158°W) and a newly established and heavily instrumented time-series mooring site K2, operated by the Japan Agency for Marine-Earth Science Technology (JAMSTEC) in the NW Pacific (47°N 160°E). Logistics and background support at both sites include appropriate physical and biogeochemical time-series observations, and deep trap moorings. These data enable us to evaluate our detailed studies of twilight zone processes in the context of the annual cycles of production and export.

Station ALOHA has been visited on average once per month since late 1988 for detailed biogeochemical studies and these cruises include regular 3-4 day deployments of shallow, 150m drifting sediment traps (Karl and Lukas, 1996). Particle flux at ALOHA is also measured at greater depths using moored time-series traps at 2800 and 4000 m. Station K2 is visited less regularly: from once to several times a year since 2001. K2 is further offshore and thus less impacted by coastal processes than the earlier Japanese time-series work in the NW Pacific at KNOT (Liu *et al.*, 2004). During the VERTIGO field year in 2005 there were cruises in March and September to turn around the K2 mooring system, which consists of an automatic water sampler to observe near-surface nutrients, an optical sensor in the euphotic layer (Honda and Watanabe, 2007) and sediment traps at 150, 540, 1000 and 4810 m. A wider suite of elements, inorganic and organic forms of carbon, pigments, natural radionuclides and primary productivity were measured during mooring deployment and retrieval cruises.

ALOHA is an oligotrophic site, characterized by warm surface and mesopelagic waters with persistently low macronutrients and correspondingly low surface chlorophyll (surface DIN fields shown in Figure 1). In contrast, K2 is a colder, mesotrophic site in the NW Pacific subarctic

gyre, with seasonally variably macronutrient concentrations and nutrient drawdown in summer in response to variability in primary production and export. The SeaWiFS satellite derived surface chlorophyll data for our VERTIGO studies in 2004 (ALOHA) and 2005 (K2) reflect these differences (Figure 2). The ALOHA cruise took place during an extended period of low and constant surface chlorophyll *a* (Chl *a*) concentrations around 0.07 mg m^{-3}. At K2 there was significant seasonal variability in surface Chl *a*, ranging from 0.15 to 0.7 mg m^{-3} and higher, with greater regional variability (note larger error bars for K2 reflect Chl *a* variability). We arrived at K2 about 20-30 days after the seasonal maximum in phytoplankton biomass in 2005, and prior to a slightly smaller autumn bloom (Figure 2). Note that satellite ocean color data are much scarcer at K2 compared with ALOHA due to extensive cloud cover. At K2 less than one-half of the available pixels are sampled within the 100 km box over the 8 day window (our averaging parameters used in Figure 2) and nearly 25% of the time, less than 10% of the 100 km box is sampled. Whereas for ALOHA, the coverage of the 100 km box is nearly complete (94% on average) and for only one 8-day composite is the coverage less than 50% for the sampling box.

Representative vertical profiles taken during VERTIGO from each site indicate a strong contrast in the physical and biogeochemical settings (Figure 3). ALOHA was warmer and saltier than K2, with a summer mixed layer (ML) of 50 m and light penetration (0.1% of surface irradiance) to approximately 125 m, the depth of the deep chlorophyll maximum (DCM). At greater depth there was a significant increase in macronutrients concentrations. K2 was much colder and fresher, with a shallower 25 m summer mixed layer above the temperature minimum of <2 ºC near 100 m. This temperature minimum forms due to winter cooling and fresh water inputs to surface waters. In the K2 mixed layer, macronutrient concentrations were all high (N ~ 12; Si ~13; P ~1.3 µM) though there was an apparent and variable drawdown of macronutrients as the season progressed (see section 3.4.). The DCM at K2 was at 50 m, again roughly the depth of the 0.1% light level;

however, during the first half of our cruise, many stations also showed a shallower and narrow peak in Chl *a* and plankton biomass at <10 m.

Major differences in plankton community structure were readily seen in pigment profiles and were confirmed by microscopic and flow cytometric analyses. Previous studies have shown that K2 is a site of high diatom biomass, evidenced here by the elevated concentrations of the diatom specific pigment fucoxanthin that correspond to both chlorophyll peaks (Figure 3). In contrast, ALOHA had low fucoxanthin concentrations, but high levels of zeaxanthin, a pigment associated with cyanobacteria (Andersen *et al.*, 1996). *Prochlorococcus* spp. the most abundant phototroph at ALOHA, were absent at K2 (Zhang *et al.*, 2007-this volume).

In terms of the annual cycles of primary production and export, we can place our flux data in context of time-series measurements at these two sites. At ALOHA time-series data showed peak primary production in 2004 during May (Figure 4), though the climatological peak in production is typically later in July, when light levels are highest (Letelier *et al.*, 1996; Karl *et al.*, 2002). As in other years, the 2004 data showed no correlation between production and POC flux as measured by 150 m drifting sediment traps during the HOT program (Figure 4). Our trap POC flux at 150 m for deployment 1 (D1) and deployment 2 (D2) averaged 1.5 mmol m^{-2} d^{-1}, which was similar to the HOT data in May (HOT #159) and August (HOT #162), but lower than the HOT cruise immediately preceding VERTIGO (HOT #160; note there were no trap data on HOT #161).

At K2, annual productivity data was not available, but the onset of the biomass increase in surface waters was evident in the SeaWiFS images (Figure 2), with peak biomass in late June. Nutrient data were obtained with a moored remote automated sampler (RAS; McLane Research Laboratories, Inc.) deployed at ~35 m (Honda and Watanabe, 2007), where a 30 μM seasonal

drawdown was found for dissolved Si (dSi) associated with diatom growth and export (Figure 4; more details on nutrient drawdown at K2 in section 3.4.). The VERTIGO 150 m POC flux data showed a significant decline during our K2 cruise, starting much higher during D1 and dropping by a factor of 3 about one week later during D2 (5.1 to 1.9 mmol m^{-2} d^{-1}). This same trend in decreasing flux at the termination of this diatom bloom was echoed in the time-series record from a deep moored trap at 4800 m, though the POC flux at depth was considerably attenuated (Honda, unpublished data). We also know this flux was associated with diatoms due to the high percent of particulate biogenic silica (bSi) in the traps, which is 80% opal (dry weight basis) at 150 m at K2 vs. <10% at the same depth at ALOHA (Buesseler *et al.*, 2007b).

3.2. Spatial and Temporal Variability at ALOHA

At ALOHA, we sampled within a mesoscale anticyclonic eddy feature with a diameter of roughly 200 km, sea level elevation of ~20 cm relative to its surrounding waters and resulting surface currents of up to 30 km d^{-1} (Figure 5). Time sequences of sea level show a slow migration of the feature to the west at a rate of ~5 km/day. CTD casts were conducted within a 10-20 km distance from the trap deployment and retrieval sites, and on larger 100-200 km surveys between deployment periods (drifting trap trajectories and central CTD stations are shown in Figure 6). The drifting traps and neutrally buoyant sediment traps generally followed the clock-wise rotation of the eddy feature. Within the spatial scales sampled during our cruise, variability in space and time within the ALOHA site was low, as evidenced by the small standard deviation in satellite-derived surface Chl *a* (Figure 2). Furthermore, within the 100 CTD casts at ALOHA there were only modest station-to-station differences in pigment biomass and a 17% decrease in Chl *a* between D1 and D2 (Figure 7; Chl *a* for D1 = 0.047 ± 0.01 and for D2 = 0.039 ± 0.01 mg m^{-3}; mean ± standard deviation for the mixed layer), as evidenced by the *in-situ* CTD-based fluorescence data, which were calibrated against discrete measurements of Chl *a* using HPLC.

During the 18 day occupation of the ALOHA site, the rates of net primary production (NPP) and new production were invariant (Boyd *et al.*, this volume; Elskens *et al.*, this volume), as well as the magnitude and composition of the sinking particle flux in the mesopelagic traps (Buesseler *et al.*, 2007b; Lamborg *et al.*, this volume-a). Filtered particle concentrations were also relatively constant as measured on four *in-situ* pump casts (data not shown), with most of the particulate carbon associated with small (>1-53 μm) rather than large (>53 μm) particles (representative profile in Figure 8). Dissolved inorganic nitrogen (DIN) in the mixed layer remained below detection (DIN = NO_3 and NO_2; detection limit here = 0.05 μM) though with more sensitive methods DIN can be measured at nanomolar concentrations at all depths (Karl *et al.*, 2001). Furthermore, HPLC pigment data and microscopic analyses documented that phytoplankton composition and biomass was relatively uniform during the course of our occupation of the site, and the DCM remained at the same density throughout this time as well. Likewise heterotrophic processes remained constant as evidenced by the zooplankton biomass and metabolism profiles as well as bacterial production in the upper 1000 m (Steinberg *et al.*, 2007).

3.3. Spatial and Temporal Variability at K2

During our 23 day occupation of the K2 site, there was considerable cloud cover that severely limited satellite detection of surface chlorophyll. In general, we do see within the annual surface color record considerable seasonal variability and high regional variability in surface chlorophyll (Figure 2). As during ALOHA, we used the CTD mounted *in-situ* fluorometer to provide a record of spatial and temporal changes in phytoplankton biomass and over a 200x200 km area as measured on over 80 CTD casts (Figure 7). These data show modest variability in chlorophyll biomass between stations, with a 25% decrease between D1 and D2 (Chl *a* for D1 = 0.34 ± 0.06, and for D2 = 0.26 ± 0.06 mg m^{-3}; mean ± standard deviation for the mixed layer). Net primary

production also decreased by about 25% between D1 and D2 at K2, with a substantial decrease in the contribution of large algal cells >20 μm to NPP (Boyd *et al.*, this volume).

The surface flow field at K2 was predominately eastward but with considerably lower velocities then observed at ALOHA (Figure 5). During the VERTIGO cruise, the K2 site was situated between two mesoscale features; a cyclonic feature to the north and an anticyclonic eddy to the south. The difference in sea level between these two mesoscale features was ~20 cm which generated an eastward geostrophic current of roughly 10 km/d.

The overall decrease in chlorophyll reflects the end of a regional diatom bloom that had peaked in biomass several weeks prior to our arrival (Figure 2). This decline in biomass was supported by mooring data and shallow trap fluxes of bSi and POC (Honda *et al.*, 2006; Honda and Watanabe, 2007). Concurrent with the drop off in surface biomass was a decrease in large particulate carbon concentrations in the shallowest samples (Figure 8).

Microscopic analyses of phytoplankton (M. Silver, unpublished data) confirmed that the high Si/organic matter content at K2 resulted from the dominance of diatoms. Three of the dominant diatoms were highly silicified species: *Chaetoceros* spp. (especially *atlantica*), *Coscinodiscus marginatus* and *neodenticula*. The former two were especially abundant in the traps as broken fragments, indicating they were heavily grazed on the surface, likely by the abundant calanoid copepods, whereas *neodenticula* tended to be intact but empty of protoplasm. The processes of intense extraction of organic matter from the diatoms, which could have involved both metazoan and protozoan grazers (ciliates were quite abundant in the euphotic zone), would have led to an unusually heavy biogenic silica flux at depth. This was confirmed by the direct measurement of a high bSi content in our traps consistent with sinking diatom debris (Buesseler *et al.*, 2007b). Furthermore, high numbers of Phaeodarian radiolarians sampled in net tows in the mesopelagic

zone at K2, and found in sediment traps, likely contributed to the high biogenic silica flux as well (Steinberg et al., this volume). We saw high and efficient transport of POC to depth at K2, suggesting not only empty tests, but that significant POM was associated with the sinking diatom and radiolarian material. A large fraction of this diatom debris in traps was found in intact fecal pellets and these pellets were estimated using food web models to account for the majority of the flux at K2 (Boyd *et al.*, this volume).

3.4 Nutrient Drawdown at K2

The macronutrient concentrations, both from the time-series nutrient sampler and the VERTIGO cruises can be used to look at the magnitude and seasonality of phytoplankton nutrient uptake and to place initial constraints on export fluxes. To first order, nutrient uptake in the ML will be balanced by increases in particulate organic forms, i.e. biomass, and/or export at depth. When comparing ML budgets to 150 m export, we attribute this change to processes between the base of the ML and the first trap at 150 m. However we should also consider changes to stocks of dissolved organic forms (for DON, which we did not measure- see 3.4.2) and vertical mixing (which is small relative to the changes in nutrient stocks).

3.4.1 Effect of diatom growth and remineralization on dissolved nitrogen and silica

The overall decrease in Chl *a* between D1 and D2 corresponded to a decrease in diatom pigments (and estimated C biomass) over time at the K2 biocast stations (Figure 9). We observed over the course of two weeks a decrease in surface fucoxanthin concentrations from 100 to 40 ng l^{-1}. The fucoxanthin decrease in the ML corresponds to a diatom removal rate of 2.5 mmol C m^{-2} d^{-1} (derived from the slope in Figure 9B). Low ratios of chlorophyllide *a* (a diatom senescence biomarker (Bidigare *et al.*, 1985) to fucoxanthin during the time-series measurements indicated

that the demise of the diatoms was not due to cellular senescence. During the same period, DIN:dSi nutrient ratios increased due to preferential removal of dSi from the surface layer. Thus sites with the lowest diatom abundance post-bloom (lowest fucoxanthin) correspond to the highest net removal rates of dSi due to diatom growth and export.

The non-diatom photosynthetic picoeukaryotes (Peuk) and *Synechococcus* spp. also decreased during this period, with corresponding C removal rates of 0.9 and 0.5 mmol C m^{-2} d^{-1}, respectively (derived from Figure 9B). Similarly, bacterial biomass decreased 16% between D1 and D2 (Zhang *et al.*, 2007, this volume). It is interesting to note that the total phytoplankton C removal rate of ~4 mmol C m^{-2} d^{-1} derived from pigments for the ML falls between the D1 and D2 measured POC flux at 150 m though processes below the ML certainly contribute to POC flux at 150 m as well. It is likely that the removal rate of non-diatom photosynthetic eukaryotes is underestimated since the Peuk population measured by flow cytometry does not include larger and rarer non-diatom photosynthetic eukaryotes (i.e. cryptophytes and dinoflagellates). Based on the concentrations of alloxanthin (cryptophyte marker) plus peridinin (dinoflagellate marker) relative to total carotenoids, non-diatom photosynthetic picoeukaryote biomass is underestimated by ~7 ± 1%. Despite the decrease in phytoplankton biomass at K2, the relative proportions of C biomass as diatom (64 ± 10%), photosynthetic Peuk (27 ± 6%) and *Synechococcus* (9 ± 4%) remained relatively constant in the upper 25 m during this period.

Considering the entire 200 x 200 km study area, the variability in DIN:dSi is larger, ranging from <1 to almost 5, and this ratio remains inversely correlated to the diatom pigment fucoxanthin (Figure 10). Thus on larger spatial scales throughout this region, the variability in diatom biomass reflects the state of the local diatom bloom, with a loss of diatoms being accompanied by preferential removal of dSi over DIN in the dissolved nutrient fields.

The same parameters, when plotted vs. density, show a remarkable coherence and clear temporal trend (Figure 11). During D1, two peaks in diatom and Chl *a* pigments were observed, one at <10 m (density = 25.3) and a second at ~50 m (DCM; density = 26.4). Between D1 (filled symbols) and D2 (open symbols), the shallow diatom peak disappeared, and it is in these waters that the corresponding increase in DIN:dSi was greatest (Figure 11, right panel). What is interesting is a "bulge", or increase in DIN:dSi just at and below the DCM, below which there was a continued decrease in DIN:dSi with increasing density. Such a vertical profile would be created by enhanced remineralization of sinking PON at these depths.

We can also examine these changes in nutrient uptake and regeneration by plotting dSi vs. DIN (Figure 12). One can immediately see that the diatoms would drawdown dSi to zero well before all of the DIN would be consumed, thus dSi, not DIN would be an ultimate macronutrient limit to the growth of diatoms at K2. However, by the end of D2, about 7-8 μM dSi still remained in surface waters, so something other than dSi limitation, must have caused the crash of this diatom bloom. The high abundance of copepods and pellets full of diatom debris certainly points to grazing controls. Also, experimental data on iron limitation and evidence of low photosynthetic efficiency at K2 (Boyd *et al.*, this volume), suggested that diatom growth was iron limited. So both top down and bottom up micronutrient controls could be responsible for the demise of the summer diatom bloom. The slope in Figure 12 is equivalent to the uptake ratio of dSi relative to DIN, at least in surface waters where nutrient uptake exceeded regeneration. The slope of dSi:DIN in the upper 55 m (down to the DCM; dSi <40 μM) is 4.0 ± 0.3. Below the DCM to about 105 m, where there is a break in slope (and where we see the bulge in dSi:DIN; Figure 11), the drawdown ratio is 1.4 ± 0.2. This slope increases again in deeper waters to 3.8 ± 0.4 (deep waters defined by dSi > 60 μM).

The slope change just below the DCM is where the system switches from being a site of net autotrophic production, with large nutrient drawdown, to one where low light levels cannot support significant production. Concentrations of dSi decreased between D1 and D2 in the upper 55 m during our occupation. We suggest that the difference between the uptake ratio around 4 and the ratio <2 below 55 m was due to shallow remineralization of N-rich labile material immediately below the DCM, as reflected by the change in slope and bulge in DIN:dSi ratio (Figure 11). This is also supported by the comparison between DIN budgets and the 150 m traps (see 3.4.2). The deeper waters matched the surface drawdown ratio of 4. The particles that sink through the mesopelagic, have particulate N:Si ratios that are even higher, ranging from 17 (D1) to 13 (D2) at 150 m and increasing with depth in K2 traps, as bSi has significantly longer remineralization length scales than N on sinking particles (Buesseler *et al.*, 2007b; Lamborg *et al.*, this volume-a). Thus, particles become relatively Si rich and N poor as they sink through the water column.

3.4.2 K2 nutrient drawdown and export fluxes

It is interesting to look at the drawdown of surface nutrients vs. the flux of sinking particles and the elemental ratios of uptake and export (Table 1). One estimate of the seasonal nutrient change is derived from the moored time-series water sampler deployed at 35 m. This device provides an estimate of the net seasonal drawdown of macronutrients for a 110-day period between the end of June and mid October (dSi data shown in Figure 4; Honda and Watanabe, 2007). A second way we can evaluate nutrient drawdown is to use the VERTIGO profiles. Assuming the winter profile is well mixed, we use the lower concentrations measured during VERTIGO above the break in nutrient concentration at the DCM as an indicator of seasonal drawdown in the upper 50 m. For this calculation, we take as a starting point in time, the end of June (just prior to drawdown seen in the nutrient time-series) and as our end point, the last VERTIGO CTD cast 40 days later in

August. A third estimate of nutrient drawdown can be derived from the changes we observed in the ML between D1 and D2, which represents the short term nutrient loss rate, and this was only measurable for dSi, as changes in N were not significant over this 10 day period. All of these nutrient budgets ignore the supply of new nutrients from below due to mixing, so are a slight underestimate, but are still informative for looking at surface drawdown vs. export fluxes and the elemental ratios of uptake and export (Table 1). These estimates also ignore build up of particulate bSi stocks, but with decreasing fucoxanthin pigments and decreasing PC (and PN) stocks in the ML (Figures 8 and 9), there is no evidence for a build up of bSi stocks or diatom biomass, but rather uptake of dissolved macronutrients and rapid loss associated with sinking particles.

If we look first at the seasonal pattern of nutrient drawdown measured with the time-series sampler, there was a depletion of 30 μM dSi and 10 μM DIN between the end of June and mid-October (after which nutrients begin to increase, presumably due to overturn and mixing in the fall; Table 1). From the vertical profiles, our 40 day estimate of nutrient depletion is of similar magnitude, and both suggest a relative dSi:DIN drawdown ratio of ~3 (molar). When calculated on a month by month basis from time-series samples, this dSi:DIN ratio dropped from a high of 4.5 in July/August, to 1.2 in September/October (data not shown). This ratio is significantly higher than the average Si:N ratio of diatoms, which is closer to 1 (Brzezinski, 1985), and supports the observation of heavily silicified diatoms. This ratio can also increase due to stresses on diatom growth, such as light, macro-, or micronutrient limitation (Hutchins and Bruland, 1998; Saito *et al.*, 2002; Sarthou *et al.*, 2005). Since the concentration of macronutrients remains well above the half saturation constants of ~1 μM for DIN and ~3 μM for dSi, we consider light or iron limitation as more likely causes for enhanced silicification (Boyd *et al.*, this volume).

In terms of nutrient budgets and flux, whether we take the long term seasonal drawdown from the time-series sampler or the 40 day estimate for upper 50 m, the predicted losses of 3-11 mmol m^{-2} d^{-1} for DIN or 9-38 mmol m^{-2} d^{-1} for dSi are much greater than observed fluxes of 0.2-0.6 mmol m^{-2} d^{-1} for DIN or 3-11 mmol m^{-2} d^{-1} for bSi found in the 150 m traps for D1 and D2. Part of this difference might be due to the fact that we are capturing the end of a diatom bloom, when fluxes are dropping off rapidly, compared to a flux derived from longer term seasonal nutrient budgets; however the high flux in the surface still holds when comparing shorter term bSi losses between D1 and D2 (see below).

The difference between the trap flux at 150 m and the nutrient budgets may tell us something about the magnitude of shallow remineralization. For example, the 150 m N trap flux/upper 50 m N drawdown is only 2-5% but 8-30% for Si (the lower estimates for both are obtained when D2 vs. D1 fluxes are used). In other words, more than 4-5 times as much sinking PON is lost between 50-150 m than bSi. This is consistent with the lower transfer efficiency (T_{eff}) between 150-500 m of N vs. Si based upon our sediment trap data (Buesseler *et al.*, 2007b) and the basic hypothesis that higher density particles reach the seafloor with higher efficiency due to faster sinking rates, and/or slower remineralization rates than more labile organic materials (Armstrong *et al.*, 2002; Francois *et al.*, 2002). The comparison is not ideal, since we are measuring flux for 3 day periods in late July/early August, and the 50 m budget is at best, a minimum estimate of the drawdown of nutrients over the initial 40 days of the growth period. So the exact magnitude may not be correct, though the preferential remineralization of N over Si is a robust, but perhaps not surprising conclusion. The trap samples have a C/N ratio of 8 or more, which also argues for more rapid remineralization of total particulate N than C (Lamborg et al., this volume-a).

A better match in time would be possible if we compared just D1 and D2 results. While DIN stocks did not change significantly between D1 and D2, dSi did continue to decrease by 10 +/- 5 μM in the ML. From this drawdown, one calculates a dSi loss on the order of 23 mmol m^{-2} d^{-1} specific to the dates of our trapping program. We measured bSi fluxes of 11 and 3 mmol m^{-2} d^{-1} during D1 and D2, respectively, or on average, 30% lower (equivalent to 70% bSi remineralized between 25 m and 150 m), but there are larger uncertainties on this short term bSi budget. Also, since we have ignored continued mixing of nutrients into the ML in our budgets, these estimates of shallow remineralization are certainly an underestimate of losses above 150 m. Alternatively using results of ^{15}N labeling experiments, we measured DIN removal fluxes of 8 and 7 mmol m^{-2} d^{-1} during D1 and D2 respectively, equivalent to about 95% particulate nitrogen remineralized and/or grazed within the upper 150 m. Based on ^{15}N, most of this shallow PN remineralization occurred in the vicinity of DCM (Elskens *et al.*, this volume). In the upper 20 to 40 m depth interval, a net production rate of ammonium was found (the sum of ammonification plus ammonium excretion by zooplankton minus the sum of nitrification and ammonium uptake), while at the DCM and just below (50 to 60 m), ammonium concentration rapidly dropped off with a net consumption rate probably reflecting nitrification processes (Elskens *et al.*, this volume). The agreement on high N remineralization from N isotopes and the surface DIN stocks and NBST fluxes, is encouraging and suggests that N is not simply building up as DON in the surface layer (not measured) or PON stocks (decreasing), but more likely is exported on sinking PON at and remineralized below the DCM.

However, there is also at least one alternative explanation why the trap fluxes are so low relative to the changing nutrient stocks. Zooplankton diel migrators feed in the surface waters and actively transport this ingested POM to depth where they can respire CO_2, excrete DOM, release pellets, and are themselves subject to carnivory and consumption by other mesopelagic

zooplankton. The observation that the mesopelagic bacterial and zooplankton carbon demand greatly exceeds (each by factors of ~2 – 10) the sinking flux of POC and its attenuation at depth (Steinberg *et al.*, 2007), could only be explained by a mesopelagic community that is being sustained by active diel migrants and surface feeding, or temporal offsets in growth (i.e. stocks) and C demand. These migrants would consume phytoplankton biomass in the surface waters and carry materials to depth that would bypass the traps. To first order, the 70% loss of bSi estimated from the ML stocks and 150 m trap fluxes may be an indicator of the magnitude of this active transport process, i.e. roughly twice as much active transport as passive sinking losses, but this ignores net losses of bSi at and below the DCM. The higher (> 90%) difference between N loss and N in the trap, at least relative to Si, would in this case be attributed to both active transport and shallow remineralization of the more labile N components of the sinking flux.

3.5. Comparison of primary production and shallow export

Many studies, such as the JGOFS program, have attempted to compare surface ocean C uptake and the export of C through the ocean to the deep sea (Lee *et al.*, 1998; Boyd and Newton, 1999; Berelson, 2001; Nelson *et al.*, 2002). We can explore similar vertical connections to the deep-ocean in VERTIGO (Figure 13). Looking first at ocean C uptake, we had excellent agreement between ^{14}C and ^{13}C deck based methods for NPP, with fairly constant conditions between D1 and D2 at ALOHA, and a 25% decrease in NPP at K2 between deployments (Boyd *et al.*, this volume). The export ratio (e-ratio) is traditionally defined as the ratio of shallow trap flux to primary production, and over appropriate time and space scales, should be similar to the f-ratio (see below), i.e. the supply of new nutrients to the surface ocean should balance shallow export fluxes (Eppley, 1989). For VERTIGO, we can calculate an e-ratio from the 150 m POC flux/integrated NPP and this equals 10% (D1) and 8% (D2) at ALOHA and 12% (D1) and 6% (D2) at K2. This similarity in e-ratio at first appears surprising given prior studies that suggest

higher e-ratios in cold water systems dominated by larger phytoplankton cells (e.g. Michaels and Silver, 1988).

One explanation for the similar e-ratios at 150 m is that the depth of the euphotic zone is much shallower at K2 (0.1% light at 50 m) vs. ALOHA (125 m). Thus while our shallowest trap is only 25 m below the euphotic zone at ALOHA, it is 100 m deeper at K2. The nutrient budgets for dissolved N discussed above (see section 3.4.2) support considerable remineralization of sinking particles at K2 below 50 m and above the 150 m trap. Thus a better comparison in terms of surface export efficiency and its relationship to the local food web, is to extrapolate POC flux to 125 m at ALOHA and to 50 m at K2, resulting in an e-ratio normalized to the depth of the euphotic zone of 13% (D1) and 11% (D2) at ALOHA and 21% (D1) and 11% (D2) at K2 (extrapolating to shallower depths is done following a Martin *et al.* 1987 fit to VERTIGO flux profiles: b= 1.33 and 0.51 for ALOHA and K2, respectively, from Buesseler *et al.*, 2007b). In fact, the relative decrease in e-ratio at K2 between D1 and D2 fits nicely with a decrease in NPP attributed to the larger (>20 μm) phytoplankton cells (Boyd *et al.*, this volume), since lower surface export efficiency is predicted with a shift to smaller cells (Michaels and Silver, 1988). However the differences in e-ratio between sites are still not as large as one might predict based upon the much higher abundance of large phytoplankton cells at K2 vs. ALOHA, and are more in line with new models that suggest a higher fraction of export associated with picoplankton (Richardson and Jackson, 2007).

Using ^{15}N-uptake experiments, we obtained f-ratios (the ratio of N_2 +NO_3 based production divided by the total N production) ranging from 22% (D1) and 17% (D2) at K2 (upper 50 m) to 20% (D1) and 27% (D2) at ALOHA (upper 100 m; Elskens *et al.*, this volume; Elskens, unpublished). At ALOHA, the constant low nitrate concentration in the upper water column and the lack of variation in the vertical profile suggest that the nitrate assimilation detected in the

upper 100 m at this oligotrophic site might have been regenerated, rather than new production. A similar assumption has been made for the oligotrophic Bermuda time-series site (Lipschultz, 2001). Ignoring nitrate assimilation at ALOHA, the f-ratio decreases on average to 12% in much better agreement with the e-ratio normalized to the depth of the euphotic zone (see above). However, consideration of the natural abundance nitrogen isotope balance in the upper 150 m at ALOHA suggests that approximately 80% of the export flux may be supported by nitrate (Casciotti *et al.*, this volume). If this is the case, much of the nitrate-supported export may be occurring in the deep chlorophyll maximum between 100-150 m (Letelier *et al.*, 1993; Fennel *et al.*, 2002), and may include inputs from vertical migration of nitrate-assimilating algae (Richardson *et al.*, 1998; Singler and Villareal, 2005). Given that new and export production need not balance on short timescales, the overall coherence of the VERTIGO observations was very good.

In addition to considering community structure in comparing export efficiencies, we also need to consider the temporal bloom dynamics. In any bloom, the onset of production will precede the increase in POC export. At K2 we have observations during the tail end of a diatom bloom when NPP has already decreased (Figure 2) and POC flux is trailing off as well (Figure 4). Therefore, the euphotic zone normalized e-ratios and f-ratios were only higher at K2 during D1, but do not represent the fractional POC export from that diatom-dominated community on a seasonal or steady state basis. Both of these issues mentioned above, changing depth of the euphotic zone and the seasonal progression of a bloom, need to be considered. Simply finding a higher or lower e-ratio and f-ratio at a single point in time does not necessarily illustrate ecosystem driven changes in net community export or the potential for C export.

As an important aside, methods also matter. VERTIGO deck based NPP incubations, at least at ALOHA, are >2 times lower than *in-situ* NPP determined one month prior/post on HOT cruises

(HOT #160 and #162), despite very similar conditions and vertical distribution of Chl *a* in the water column during VERTIGO and the HOT cruises. The VERTIGO NPP are lower because they are based on 24 hour incubations thus they include night time respiration, while HOT reports primary production for the 12 hour light period only. Part of this difference may also be attributed to deck vs. *in-situ* based NPP (Boyd *et al.*, this volume), similar to what has been seen in a past study at ALOHA where deck based methods are much lower than the *in-situ* NPP values (Karl *et al.*, 1996). With similar trap fluxes and higher NPP, the average HOT based e-ratio for 2004 is 5 ± 2% (mean ± st. dev. from HOT data as shown in Figure 4), with a long term average e-ratio of 7% (for 1988-1993 with a reported range of 2-17%; Karl *et al.* 1996). It is noted that the differences in NPP between HOT and VERTIGO cruises do not influence our f-ratio estimates based on ^{15}N tracer techniques, but will impact our new production rates ("exportable production") calculated as the product f-ratio times NPP. Under these conditions the exportable production at K2 would be greater than ALOHA, but only for D1 (Elskens *et al.*, this volume and unpublished data from ALOHA).

3.6. Comparison of mesopelagic and deep trap fluxes

Extending the comparison of C fluxes below the 500 m trap to deep moored traps to examine deep-ocean transfer efficiency is also not as straight forward as one might expect. There are important issues to consider, including: 1) the time-lag between shallow and deep flux; 2) differences in trap collection efficiencies; and 3) differences in the source funnel or collection area for the traps. Looking first at the time lag issues, these are most important when the shallow and/or deep fluxes are changing. At ALOHA the mesopelagic fluxes were constant; at 500 m the value for POC was 0.3 mmol m^{-2} d^{-1} for D1 (June 23 - 28) and D2 (July 2 - 7). At 4000 m, Karl et al. (unpublished results) see an increase in the July 31 – Aug. 16 deep trap POC flux to 0.36 mmol m^{-2} d^{-1}, after a period of several months of near constant flux of about 0.2 mmol m^{-2} d^{-1}.

Comparing the constant flux period through July 30th gives us a deep POC transfer efficiency (flux 4000/500 m) of 66% (calculated using June 26 – July 30 avg. flux at 4000m), or up to 84% if you consider that the shallow material is still falling directly into the deep trap that opened on July 31 (calculated using June 26 – Aug. 16 avg. flux at 4000 m). If surface fluxes are constant and the deep flux is increasing, one must assume that the deep-ocean transfer efficiency has increased for some reason if we consider an arrival time at depth later than July 31st. Taken together with the VERTIGO mesopelagic transfer efficiency (flux 500/150 m), the results suggest that the majority of the POC flux at ALOHA is attenuated in the mesopelagic (80% decrease between 150 and 500 m) and much less below in the deep-ocean (an additional 20-40% decrease between 500 and 4000 m), for a total transfer efficiency of POC between 150 and 4000 m of about 10%. This summer time ratio is slightly greater than the HOT average over the entire year, where for 2004, the POC flux at 4000/150 m was 0.07 ± 0.04 (using the deep trap 2004 average and HOT 150 m drifting traps for 2004).

The story is more complicated at K2, where temporal dynamics in POC flux were greater, with decreasing fluxes in both shallow and deeper traps during our cruise (Figure 4). At K2, the decreasing flux at depth mirrors and lags the surface NPP and shallow flux decreases (Honda *et al.*, 2006). Our 500 m POC fluxes were 2.4 (July 30 – Aug. 4) and 1.1 (Aug. 10-15) mmol m^{-2} d^{-1} and 4800 m POC fluxes in the same units dropped from 1.4 (Aug. 6-19) to 0.7 (Aug. 20-Sept. 2) and 0.34 (Sept. 3-29). During VERTIGO, we estimated that > 60% of the POC at K2 was sinking at rates >140 m d^{-1} (Trull *et al.*, this volume). Honda (unpublished data) use peak matching of shallow and deep trap fluxes to estimate sinking rates ranging from roughly 150 to 300 m d^{-1} between 1000 and 4800 m. If we assume that the 500 m material would have reached these 3 deep trap cups in 15-30 days, the K2 deep POC transfer efficiency (flux 4800/500 m) would be 44 to 57% (assuming D1 material fell into deep trap cups spanning Aug. 6 – Sept 2, or D2 material fell into deep trap cups spanning Aug. 20- Sept. 29). By this calculation, about half

of the material that exits the 500 m horizon reaches the deep trap, which is somewhat less than ALOHA. However, this comparison is very sensitive to the chosen time lag for delivery to depth.

When comparing traps at different depths and of differing designs, one should also consider complications due to trapping efficiencies (Buesseler, 1991; Scholten *et al.*, 2001; Yu *et al.*, 2001). For K2, Honda (unpublished data) show using ^{230}Th and ^{231}Pa data that the deep trap collection efficiency lies between 37-51%. There are questions as to whether or not a radionuclide derived calibration applies directly to that particular radionuclide alone or to POC and all components of the sinking flux (Buesseler *et al.*, 2007a). If it does, then to the first order, a corrected deep trap flux should be two times higher for all flux components and implies that essentially 100% of the POC leaving 500 m reaches 4800 m at K2 (assuming the efficiency of a NBST is 100%, something that is supported using VERTIGO ^{234}Th data- Pike *et al.* 2006). An alternative is that distant lateral sources supply the deep trap with POC flux from a higher productivity region (discussed further below). With regard to this calibration, we do not have ^{230}Th and ^{231}Pa results from ALOHA, so we cannot make the same comparison.

The third issue to consider when comparing vertical C fluxes, is the extent to which deep traps integrate flux over a larger area, or source "funnel", compared to shallow traps (Siegel *et al.*, 1990; Siegel and Deuser, 1997). In effect, the shallower the trap and/or faster the sinking rate, the smaller the possible area from which particles may have originated. For example, a moored trap at 4000 m, collects material in any single trap cup from a source area that may be many 100's km distant from the trap itself, depending upon the flow field and mean particle sinking rates. This is important of course if the characteristics of the source region vary in the magnitude of the flux or the character of the sinking material. Siegel *et al.* (2007) have calculated particle source funnels for VERTIGO cruises at ALOHA. For the shallow 150 to 500 m NBSTs and Clap traps, all of the source funnels lie within scale of less than 60 km which, at the time of our sampling, is

a region of relatively constant surface properties. However an analyses of the VERTIGO source funnels suggests that the deep moored traps at ALOHA are likely collecting sinking particles during the course of our cruise which originated 200 km west of ALOHA (Siegel *et al.*, 2007). This western particle source region for the 4000 m trap had similar surface chlorophyll at HOT, as tracked by SeaWiFS (<5% difference; Siegel *et al.* 2007). Thus, while we cannot interpret flux below ALOHA as resulting from only 1-D vertical processes alone, this analyses does not suggest an obvious temporal change in phytoplankton biomass in the western source region that might have accounted for the increase in flux at depth in late July.

For K2, we have much less information on the velocity field above the traps required to make similar estimates for particle source funnels. Using surface altimetry and limited ADCP data, likely particle source funnels for the 150 to 500 m NBSTs are up to 40 km west and 20-40 km north (D1) or 20-40 km south (D2) (D. Siegel, personal communication). The exact determination of shallow trap particle source regions is limited by the lack of quality ADCP data. For the deep trap there are no local velocity data required to define source funnel locations, but distances would scale to a few 100 km for particles sinking 50-200 m d^{-1}. Due to the rapid link between surface nutrient uptake, primary production measured on moored instruments and deep-ocean fluxes, Honda *et al.* (2006) argue that to first order, K2 deep trap fluxes can be interpreted in a 1-D vertical manner. However, we also know from other data that there are important lateral sources of suspended particles from the margins to the VERTIGO mesopelagic traps, at least for some redox sensitive trace metals (Fe, Mn; Lam and Bishop, 2007). There were higher surface chlorophyll concentrations during our cruise several hundred km to the west of K2, south of Kamchatka (Figure 14). So to what degree a 1-D connection can be made between surface processes and deep trap fluxes will also depend upon the element in question and their potential distant sources. Certainly, the possibility for POC input from distant sources for the deep traps at K2 cannot be ignored.

3. SUMMARY and CONCLUSIONS

VERTIGO set out to study controls on the magnitude and efficiency of particle transport between the surface and deep-ocean. We picked two contrasting sites where our data could be interpreted in the context of prior studies and on-going time-series sampling. Indeed, satellite and ship-based estimates of the physical, biological and geochemical setting show large differences between the two sites in the surface communities and associated particles that are produced in the euphotic zone. ALOHA is an oligotrophic site characterized by warmer waters, persistently low nutrients, low Chl *a* concentrations, and is dominated by smaller phytoplankton species with a deep (125 m) DCM. K2 is a mesotrophic site in the NW Pacific that is much colder, has lower oxygen throughout the mesopelagic and has high surface macronutrients which become depleted as the summer diatom bloom progresses. K2 showed large temporal and spatial gradients in nutrients and diatom pigments associated with the termination of this diatom bloom. We used these changes in nutrient fields at K2 to suggest significant shallow remineralization above our shallowest trap at 150 m, and/or enhanced surface nutrient drawdown that is not balanced by sinking particles alone, but also by active transport by vertically migrating zooplankton.

The relative rates of C uptake and its transport through the mesopelagic are of interest when parameterizing the role of the biological pump in C transport to the deep sea. These connections seem direct and in most studies are interpreted as a 1-D steady state process. However, as we have discussed, differences in the depth of the euphotic zone, methods-related differences in determining C uptake and correcting trap C fluxes, the temporal variability in NPP and flux, and the 3-D nature of ocean processes make it difficult to interpret change in context of a local 1-D balance. In our data, the fraction of NPP that leaves the euphotic zone at K2 is greater than ALOHA, but only for D1 and when we adjust for the difference in euphotic zone depths (20%,

vs. 10% for K2 D1 vs. D2 and 10% for both ALOHA deployments). The interpretation of this in terms of a food web process (e.g. Michaels and Silver, 1988) is complicated by the temporal dynamics at K2. Below 500 m, both sites lose about half of the sinking POC by >4000 m, but this comparison is limited in that fluxes at depth may have both a local and distant component (Siegel and Deuser, 1997; Siegel *et al.*, 2007), and the fluxes change with time, complicating comparison over shorter time periods. The bottom line is still that the greatest difference in C flux attenuation is in the mesopelagic, here measured with NBSTs at depths of 150, 300 and 500 m (Buesseler *et al.*, 2007b).

A primary finding from VERTIGO is that the T_{eff} in the mesopelagic (POC flux 500 m/150 m) is much greater at K2 than ALOHA (Buesseler *et al.*, 2007b) and thus the hypothesis that flux attenuation is constant in the ocean can be rejected. This should not be surprising, as even within the earlier "open ocean composite" flux curve used to describe the extensive VERTEX trap data ($F = F_{100}(z/100)^{-b}$, where F_{100} = 4.2 mmol C m^{-2} d^{-1} and b = 0.86) there is considerable variability in attenuation between sites (b = 0.64 to 0.97; Martin *et al.*, 1987). More recently, the analyses of deep trap data have confirmed this variability in "b", and have led to the suggestion of carbonate ballast or sinking rate controls on particle export efficiency (Armstrong *et al.*, 2002; Francois *et al.*, 2002; Klaas and Archer, 2002; Lutz *et al.*, 2002). However, our data do not support a primary role for carbonate in controlling mesopelagic or deep-ocean POC flux, since at least at K2, the "silicate pump" appears to lead to enhanced POC delivery to the deep sea.

The reasons for this difference in mesopelagic T_{eff} are not likely to be attributable to any single process or captured in a traditional model of flux vs. depth. In the surface layer, we can predict the extent of shallow export based upon size-partitioning of NPP and the decrease at K2 in export from D1 to D2 corresponds to a shift to smaller phytoplankton cells (Boyd *et al.*, this volume). If upwelling of NO_3 is not a significant source of new nutrient at ALOHA, f-ratios and e-ratios are

in much better agreement and lower than at K2, especially for D1 (Elskens *et al.*, this volume). Pigment data shown here and microscopic analyses (M. Silver, unpublished data) clearly showed a predominance of large diatoms at K2 especially in the ML where dSi was depleted much faster than N, leading to a bSi rich flux. At K2, colder waters, lower oxygen below 150 m and heavier ballasted particles could all lead to higher T_{eff}. Interestingly the in-situ particle settling velocities measured in one experiment showed little difference between these sites (Trull *et al.*, this volume), so sinking rates alone may not be as important as particle characteristics and other processes in setting T_{eff}. By several measures, including the use of barium excess as a remineralization proxy (Dehairs *et al.*, this volume), remineralization occurred shallower at ALOHA than K2, consistent with rapid flux attenuation at ALOHA.

At K2, there was also a higher biomass of diel migrating zooplankton as compared to ALOHA. These migrating zooplankton are meeting their C demand by feeding at the surface at night and carrying C and associated elements to depth where C is either excreted, released as fecal matter, and/or these migrators are themselves consumed or die to become part of the sinking C supply to the mesopelagic and deep ocean (Steinberg *et al.*, this volume; Wilson *et al.*, this volume). These processes can enhance, rather than attenuate observed fluxes at depth. Zooplankton processes are particularly important at K2, where seasonally a high biomass of large *Neocalanus* spp. copepods undergo an ontogenetic vertical migration, going into diapause and subsequently dying at depth, resulting in a substantial transfer of C biomass to the mesopelagic that would not be caught in our traps (Kobari *et al.*, this volume). This phenomenon does not occur at ALOHA. At both sites, fecal pellets play an important role as the carrier of sinking POC and other materials to depth (Ebersbach *et al.*, 2006; Boyd *et al.*, this volume) so much of the transport efficiency at both sites may be set by the characteristics of sinking pellets formed both in surface layers (ALOHA and K2) as well as de-novo production of fecal pellets in the mesopelagic (more prevalent at K2; Wilson *et al.*, this volume). Indeed, the significantly larger zooplankton (Steinberg et al. this

volume), and larger (and thus more likely rapidly sinking) fecal pellets in traps at K2 (Wilson et al. this volume), point to the role of zooplankton community structure in increasing particle transfer efficiency at K2.

In addition to the vertical components of flux and processes directly above the trap, lateral sources of particles must be considered (Siegel *et al.*, 2007). This is especially important for sinking particles reaching deeper traps that may originate several 100 km distant from the point directly above the trap. At K2, the decrease in bSi and POC seen in the surface traps is reflected rapidly in moored traps below. However, at least some trace metals in K2 traps appear to have a margin source (Lam and Bishop, 2007). This leads to an interesting trend of decreases in POC, PON and other biogenic or labile flux components at K2, and increasing flux with depth for Fe and Mn and other trace elements (Lamborg *et al.*, this volume-b). Suspended particle feeders (Wilson *et al.*, this volume) or physical aggregation processes can enhance flux if there are lateral sources of suspended materials above the traps. Thus rather than thinking of particle flux attenuation as a single process that can be parameterized with one variable, we contend that at least three types of processes must be considered: 1) heterotrophic degradation of passively sinking material; 2) zooplankton migration and surface feeding; 3) and input from lateral sources. These three processes will need further study to unravel the mysteries of the twilight zone.

The rates and controls on particle transport through the twilight zone are important for many reasons. Sinking particles provide a rapid link between surface and deep-ocean, and many elements, including C, biominerals and associated trace elements “hitch a ride” to the deep sea. This C flux provides a food source for the mesopelagic and deep sea communities. Variability in this flux is to be expected, since many of the processes that determine the composition and internal transformations of sinking material are biological in nature, and thus respond to physical and geochemical forces that vary with space and time in the oceans. If the upwelling of nutrients

and dissolved inorganic carbon were simply balanced by local particle export in constant proportions, then the biological pump would have no impact on atmospheric CO_2 and hence climate. If however, the fluxes of POC are large and variable, as we measure, then the ocean need not be in steady state with respect to C sequestration via the biological pump, and shifts in the efficiency of this pump can have large impacts on global C balances (Buesseler *et al.*, 2007b). We already know from deep trap data that interannual variability in deep-ocean C fluxes is common. Thus it behooves us to further our understanding of the twilight zone to capture the processes that drive such large variability in the global C cycle.

ACKNOWLEDGMENTS

We thank the officers, crew and shore based support teams for the R/V Kilo Moana (2004) and R/V Roger Revelle (2005). Funding for VERTIGO was provided primarily by research grants from the US National Science Foundation Programs in Chemical and Biological Oceanography (KOB, CHL, MWS, DKS, DAS). Additional US and non-US grants included: US Department of Energy, Office of Science, Biological and Environmental Research Program under Contract No. DE-AC02-05CH11231 (JKBB); the Gordon and Betty Moore Foundation (DMK); the Australian Cooperative Research Centre program and Australian Antarctic Division (TWT); Chinese NSFC and MOST programs (NZJ); Research Foundation Flanders and Vrije Universiteit Brussel (FD, ME); JAMSTEC (MCH); New Zealand Public Good Science Foundation (PWB); and internal WHOI sources and a contribution from the John Aure and Cathryn Ann Hansen Buesseler Foundation (KOB). A number of individuals at sea and on shore, helped make the VERTIGO project a success, including: J. Andrews, C. Bertrand, R. Bidigare III, S. Bray, K. Casciotti, M. Charette, R. Condon, J. Cope, E. Fields, M. Gall, M. Gonneea, P. Henderson, T. Kobari, D. Kunz, S. Saitoh, S. Manganini, C. Moy, S. Okamoto, S. Pike, L. Robertson, D. Ruddick and Y. Zhang. Suggestions by three anonymous reviewers and help by the editor, R. Lampitt, are also greatly appreciated.

Table 1. Buesseler et al.

Changes in Surface Nutrient concentrations, derived fluxes and NBST flux at K2

		ΔDIN[a]	**± st dev.**	**ΔdSi[a]**	**± st dev**	**PON[b] flux**	**±st dev.**	**bSi[b] flux**	**± st dev.**
	Time period	**µM**		**µM**		**mmol m^{-2} d^{-1}**		**mmol m^{-2} d^{-1}**	
Moored time-series[c]	*June 28- Oct. 17*	10.6	0.7	29.6	0.9	3.4	0.2	9.3	0.3
Profiles[d]	*June 28 – Aug. 7*	9.3	1.8	30.2	3.2	11.7	2.2	37.7	4.0
D2 – D1[e]	*Aug. 1-12*	bd		9.5	5.2	bd		22.8	12.5
NBST D1[f]	*July 30 – Aug. 2*					0.6	0.08	11	0.5
NBST D2[f]	*Aug. 10 – 13*					0.2	0.02	2.9	0.5

a. Changes in concentration for given time period and depth interval
b. Particulate fluxes derived from concentration changes or as measured in NBSTs
c. Data from moored nutrient sampler over a 110 day time period and extrapolated to upper 35m (depth of sampler)
d. Data from moored nutrient sampler on June 28th relative to final nutrient profile collected during VERTIGO on Aug. 7th (40 d later) extrapolated for the upper mixed layer (0-25m).
e. Data from early and late VERTIGO occupations of K2. During this period (10.4 d) measurable changes in DIN were not observed (bd) and hence PON fluxes could not be calculated.
f. NBST fluxes at 150m for D1 and D2 as reported in Buesseler *et al.*, 2007b and Lamborg *et al.*, this volume-a.

Figure Captions

Figure 1. Map of North Pacific showing the locations of VERTIGO sampling sites at ALOHA and K2. Average surface DIN concentrations (μM) are contoured using Ocean Data View using data from U.S. NODC World Ocean Atlas, 2005.

Figure 2. SeaWiFS derived surface chlorophyll concentrations for 2004 at ALOHA (upper panel) and 2005 at K2 (lower panel) with dates of VERTIGO cruises indicated for comparison to the annual cycle. Data points are the mean and standard deviation of the SeaWiFS ocean color product averaged over 8 days and for a 100 x 100 km area centered on the two study sites.

Figure 3. Vertical profiles of conditions at ALOHA (circles) and K2 (triangles) during VERTIGO. Data are from bottle depths for a representative VERTIGO CTD cast in the center of our study area as follows: ALOHA = CTD 19 (O_2 data from HOT cruise); K2 = CTD 23 and CTD 24 (used for nutrients). Pigment samples (2-4 L) were filtered and LN_2 frozen at sea, and analyzed in the laboratory by HPLC (Bidigare *et al.*, 2005). Chlorophyll *a* (Chl *a*) is the sum of mono- plus divinyl-chlorophyll *a*, and fucoxanthin and zeaxanthin are taxon-specific markers for diatoms and cyanobacteria (primarily *Synechococcus* spp., based on flow cytometry and epifluorescence microscopy) respectively. Trap depths of 150, 300 and 500 m are noted by horizontal lines.

Figure 4. Selection of time-series data for 2004 at ALOHA (upper panel) and 2005 for K2 (lower panel) superimposed on the average Deployment 1 (D2) and 2 (D2) NBST POC fluxes at 150 m measured during VERTIGO (inverted grey triangles; right X-axis). In the upper panel, HOT primary productivity is plotted (filled circles; left X-axis, *in-situ* 12 hour incubations), along with 150 m POC flux measured on 3-4 day deployments using standard drifting traps (gray triangles; right X-axis; all data taken from "HOT-DOGS" data system). In lower panel, the seasonal drawdown of dissolved Si at K2 is plotted (open circles) from the time-series nutrient sampler (Honda and Watanabe, 2007), as well as the POC flux caught in the 4800 m moored time-series trap (grey bars; right X-axis; 14 day collection intervals, Honda unpublished data).

Figure 5. Maps of surface sea level elevation (color shading) and surface currents (arrows- 25 km d^{-1} scale shown) for ALOHA and K2 for the two deployment periods. The area that includes our sediment trap drift tracks and hence the most extensive field sampling is indicated by the box, which is taken from the latitude and longitude boundaries used in Figure 6.

Figure 6. Map of drifting sediment trap trajectories, deployment and retrieval sites for NBSTs and locations of central CTD stations. These are shown for each of two deployments during the VERTIGO occupation of ALOHA in 2004 and K2 in 2005. Multiple NBST deployments are identified by the following symbols: 150 m NBSTs are black triangles, 300 m NBSTs are gray circles, 500 m NBSTs are white diamonds. Trajectories of the Clap trap surface buoy are shown as follows: dashed black line-150 m trap; solid black line- 300 m trap; dark gray- 500 m trap. Trajectories for an in-situ particle sinking rate trap (Trull *et al.*, this volume) are shown as a light gray line as deployed on ALOHA D2 and at K2. CTD stations occupied during trap deployments are indicated by letters and correspond to the following legend:
ALOHA D1: A= 19, 20 B= 21,26,27,28,31 C= 22,35 D= 23,36 E= 24,37 F= 25,38 G= 29 H= 30 I= 32 J= 33 K= 34 L= 45 M= 46 N= 47 0= 48.
ALOHA D2: A= 74,79,81,82,83,84,94,96 B= 75 C=76 D=77 E=78 F=85 G=86 H=87 I=88 J= 89,90,95,96 K=91
K2 D1: A= 17,18,19,20,21,22,23,24,28 B= 25 C= 26 D= 27,31,35 E=29 F=30 G=32 H= 33 I= 36

K2 D2: A= 59 B= 62,63,64,65,66,67,68 C=69 D=70 E=72,73 G= 75 H= 76 I=77
Note that overlapping CTD stations have been combined into one identifier. Full CTD and bottle data available on line at http://ocb.whoi.edu/vertigo.html .

Figure 7. Average upper ocean chlorophyll *a* concentrations for ALOHA (upper 40 m) and K2 (upper 25 m) derived from the CTD fluorometer and calibrated against HPLC total Chl *a* concentrations. The data are shown sequentially by CTD number, thus as an approximate time-series (partial listing of CTD locations in Fig. 5; full data set on line at http://ocb.whoi.edu/vertigo.html). In each case, the central CTD "biocasts" where major biological and geochemical data were collected are shown as white bars as follows: ALOHA biocasts = CTD# 19, 27/28, 33, 45, 79, 83/84, 95, 99/100 (the "doubles" are two back-to-back CTD's at same station). K2 biocasts = CTD# 18, 23, 31, 39, 62, 66, 76, 84. The corresponding timing of the two trap deployments is indicated above the appropriate CTD numbers for D1 and D2. In general, pre and post each trap deployment, a larger scale CTD survey grid was sampled.

Figure 8. Representative profiles for the concentration of suspended particulate carbon (PC-includes PIC, but mostly POC) vs. depth at ALOHA (filled triangles; MULVFS cast 1) and K2 D1 (open circles; MULVFS cast 7) and K2 D2 (filled circles; MULVFS cast 9). Left panel shows data for PC caught on a pair of 1 micron nominal pore size quartz (QMA) filters. The PC measured on the top and bottom QMA were added, and both were down stream from a screen with a 53 µm sieve size. Right panel for fewer depths, shows PC on the >53 µm fraction (for K2, this is specific to >53-350 µm as a 350 µm pre-screen was used). Complete data can be found in Bishop *et al.*, 2008.

Figure 9. A. Time-series plots for selected K2 biocasts (CTD # 18, 23, 31, 39, 62, 76): A. DIN:dSi ratio in the upper 10 m (gray triangles; mol:mol) and fucoxanthin pigments (filled circles; ng l^{-1}) and B. diatom (filled circles; µg C l^{-1}), non-diatom photosynthetic eukaryote (gray diamonds; µg C l^{-1}) and *Synechococcus* spp. (filled squares; µg C l^{-1}) biomass in the upper 25 m. Diatom biomass was estimated using a fucoxanthin algorithm (µg diatom C l^{-1} = 0.288 * ng fucoxanthin l^{-1} - 0.012; R^2 = 0.713 and n = 130) derived from pigment and biovolume measurements (Brown *et al.*, 2007) during E-Flux III (Benitez-Nelson *et al.*, 2007) and from outside the iron-fertilized patch in SOFeX (Coale *et al.*, 2004) where similar diatom assemblages were observed. The biomass of non-diatom photosynthetic picoeukaryotes ("Peuks") and *Synechococcus* spp. ("Syn") were estimated from flow cytometry abundance measurements (Jiao *et al.*, 2002). HPLC pigment analysis revealed that the "Peuks" were dominated by haptophytes (19'-hexanoyloxyfucoxanthin) and pelagophytes (19'-butanoyloxyfucoxanthin).

Figure 10. Plot for all VERTIGO K2 stations where data were available in upper 20 m for both the DIN:dSi ratio (molar) and fucoxanthin pigment concentration (ng l^{-1}).

Figure 11. Property vs. density plot at K2 for fucoxanthin pigment (left panel; ng l^{-1}), total chlorophyll *a* (center panel; ng l^{-1}) and DIN:dSi ratio (molar; data in right panel from same station, but not always from same bottle). Early CTD's during D1 are filled circles and later CTD's during D2 are open triangles.

Figure 12. DIN vs. dSi (both in molar units) for the same stations as in Figure 9. Samples from the surface to the DCM at a depth ~55 m (dSi < 40 µM) are filled triangles; samples from below the DCM to ~105 m (dSi 40-60 µM) are open circles; samples deeper than 105 m (dSi > 60 µM) are also filled triangles. Linear regression shown for each of the 3 depth intervals as discussed in text.

Figure 13. Carbon flux or uptake vs. depth for ALOHA (left panel) and K2 (right panel), all in units of mmol m^{-2} d^{-1}. Plotted at the surface are rates of net primary production (^{14}C deck based incubations) during D1 (white stars) and D2 (black filled stars). At 150, 300 and 500 m are the average POC fluxes from the NBSTs for D1 (white) and D2 (black). The NBST 3-5 day deployments began on June 23 (D1) and July 2, 2004 (D2) at ALOHA, and July 30 (D1) and Aug. 10, 2005 (D2) at K2. The average deep trap POC fluxes at 2800 and 4000 m for ALOHA are for the period June 26 – July 30, 2004 (gray triangles). The average K2 deep trap POC fluxes at 4800 m are for Aug. 7 – Sept. 3, 2005 (gray circle). The average 0.1% light level is indicated by the dashed horizontal line at 125 m (ALOHA) and 50 m (K2).

Figure 14. Mean chlorophyll *a* surface concentrations and geostrophic currents in the larger NW Pacific region for July 2005. Areas in black have no surface Chl *a* data due to cloud cover interference with SeaWiFS images during that month.

References

Andersen, R.A., Bidigare, R.R., Keller, M.D., Latasa, M., 1996. A comparison of HPLC pigment signatures and electron microscopic observations for oligotrophic waters of the North Atlantic and Pacific Oceans. Deep-Sea Research II 43 (2-3), 517-537.

Antia, A.N., Koeve, W., Fischer, G., Blanz, T., Schulz-Bull, D., Scholten, J., Neuer, S., Kremling, K., Kuss, J., Peinert, R., Hebbeln, D., Bathmann, U., Conte, M., Fehner, U., Zeitzschel, B., 2001. Basin-wide particulate carbon flux in the Atlantic Ocean: regional export patterns and potential for atmospheric CO_2 sequestration. Global Biogechemical Cycles 15(4), 845-862.

Antia, A.N., von Bodingen, B., Peinert, R., 1999. Particle flux across the mid-European continental margin. Deep-Sea Research I 46 (12), 1999-2024.

Armstrong, R.A., Lee, C., Hedges, J.I., Honjo, S., Wakeham, S.G., 2002. A new, mechanistic model for organic carbon fluxes in the ocean based on the quantitative association of POC with ballast minerals. Deep-Sea Research II 49(1-3), 219-236.

Benitez-Nelson, C.R., Bidigare, R.R., Dickey, T., Landry, M.R., Leonard, C.L., Brown, S.L., Nencioli, F., Rii, Y.M., Maiti, K., Becker, J.W., Bibby, T.S., Black, W., Carlson, C., Chen, F., Kuwahara, V.S., Mahaffey, C., McAndrew, P.M., Quay, P.D., Rappé, M.S., Selph, K.E., Simmons, M.E., Yang, E.J., 2007. Mesoscale eddies drive increased silica export in the subtropical Pacific Ocean. Science 316, 1017-1021.

Berelson, W.M., 2001. The flux of particulate organic carbon into the ocean interior: A comparison of four U.S. JGOFS regional studies. Oceanography 14(4), 59-67.

Berelson, W.M., Balch, W.M., Najjar, R., Feely, R.A., Sabine, C., Lee, K., 2007. Relating estimates of CaCO3 production, export, and dissolution in the water column to measurements of CaCO3 rain into sediment traps and dissolution on the sea floor: A revised global carbonate budget. Global Biogeochemical Cycles 21 (1).

Bidigare, R.R., Kennicutt II, M.C., Brooks, J.M., 1985. Rapid determination of chlorophyll and their degredation products by high-performance liquid chromatography. Limnol. Oceanogr. 30 (2), 432-435.

Bidigare, R.R., Van Heukelem, L., Trees, C.C., 2005. Analysis of algal pigments by high-performance liquid chromatography. In: Andersen, R.A. (Ed.), Algal Culturing Techniques. Academic Press, New York, pp. 327-345.

Bishop, J.K.B., Schupak, D., Sherrell, R. M., Conte, M., 1985. A multiple-unit-large-volume in situ filtration system for sampling oceanic particulate matter in mesoscale environments. In: Zirno, A. (Ed.), Mapping strategies in chemical oceanography. The American Chemical Society, pp. 155-175.

Bishop, J.K.B., Wood, T.J., 2008. Particulate Matter Chemistry and Dynamics in the Twilight Zone at VERTIGO ALOHA and K2 sites. Deep Sea Research I, submitted.

Boyd, P.W., Gall, M.P., Silver, M.W., Bishop, J. K.B., 2008. Quantifying the surface-subsurface biogeochemical coupling during the VERTIGO ALOHA and K2 studies. Deep Sea Research II, this volume.

Boyd, P.W., Newton, P.P., 1999. Does planktonic community structure determine downward particulate organic carbon flux in different oceanic provinces. Deep-Sea Research I 46 (1), 63-91.

Boyd, P.W., Sherry, N.D., Berges, J.A., Bishop, J.K.B., Calvert, S.E., Charette, M.A., Giovannoni, S.J., Goldblatt, R., Harrison, P.J., Moran, S.B., Roy, S., Soon, M., Strom, S., Thibault, D., Vergin, K.L., Whitney, F.A., Wong, C.S., 1999. Transformations of biogenic particulates from the pelagic to the deep ocean realm. Deep-Sea Research II 46 (11-12), 2761-2792.

Brown, S.L., Landry, M.R., Selph, K.E., Yang, E.J., Rii, Y., Bidigare, R.R., 2007. Diatoms in the desert. Deep Sea Research II, in revision.

Brzezinski, M.A., 1985. The Si:C:N ratio of marine diatoms: Interspecific variability and the effect of some environmental variables. Journal of Phycology 21 (3), 347-357.

Buesseler, K.O., 1991. Do upper-ocean sediment traps provide an accurate record of particle flux? Nature 353, 420-423.

Buesseler, K.O., Antia, A.N., Chen, M., Fowler, S.W., Gardner, W.D., Gustafsson, O., Harada, K., Michaels, A.F., Rutgers van der Loeff, M., Sarin, M., Steinberg, D.K., Trull, T.W., 2007a. An assessment of the use of sediment traps for estimating upper ocean particle fluxes. Journal of Marine Research 65 (3), 345-416.

Buesseler, K.O., Lamborg, C.H., Boyd, P.W., Lam, P.J., Trull, T.W., Bidigare, R.R., Bishop, J.K.B., Casciotti, K.L., Dehairs, F., Elskens, M., Honda, M., Karl, D.M., Siegel, D.A., Silver, M.W., Steinberg, D.K., Valdes, J., Van Mooy, B., Wilson, S., 2007b. Revisiting carbon flux through the ocean's twilight zone. Science 316, 567-570.

Casciotti, K.L., Glover, D., Trull, T., Davies, D., 2008. Constraints on Nitrogen Cycling at the Subtropical North Pacific Station ALOHA from Isotopic Measurements of Nitrate and Particulate Nitrogen. Deep-Sea Resarch II, this volume.

Coale, K.H., Johnson, K.S., Chavez, F.P., Buesseler, K.O., Barber, R.T., Brzezinski, M.A., Cochlan, W.P., Millero, F.J., Falkowski, P.G., Bauer, J.E., Wanninkhof, R.H., Kudela, R.M., Altabet, M.A., Hales, B.E., Takahashi, T., Landry, M.R., Bidigare, R.R., Wang, X., Chase, Z., Strutton, P.G., Friederich, G.E., Gorbunov, M.Y., Lance, V.P., Hilting, A.K., Hiscock, M.R., Demerest, M., Hiscock, W.T., Sullivan, K.A., Tanner, S.J., Gordon, R.M., Hunter, C.L., Elrod, V.A., Fitzwater, S.E., Jones, J.L., Tozzi, S., Koblizek,

M., Roberts, A.E., Herndon, J., Brewster, J., Ladizinsky, N., Smith, G., Cooper, D., Timothy, D., Brown, S.L., Selph, K.E., Sheridan, C.C., Twining, B.S., Johnson, Z., 2004. Southern Ocean Iron Enrichment Experiment (SOFeX): Carbon Cycling in High- and Low-Si Waters. Science 304, 408-414.

Conte, M.H., Ralph, N., Ross, E.H., 2001. Seasonal and interannual variability in deep ocean particle fluxes at the Oceanic Flux Program (OFP)/Bermuda Atlantic Time Series (BATS) site near Bermuda. Deep-Sea Research II 48 (8-9), 1471-1505.

Dehairs, F., Jacquet, S., Savoye, N., Van Mooy, B.A.S., Buesseler, K., Bishop, J.K., Lamborg, C., Elskens, M., Baeyens, W., Boyd, P., Casciotti, K.L., Monnin, C., 2008. Barium in Twilight Zone suspended matter as a proxy for particulate organic carbon remineralization: Results for the North Pacific. Deep Sea Research II, this volume.

Deuser, W.G., 1986. Seasonal and interannual variations in deep-water particle fluxes in the Sargasso Sea and their relation to surface hydrography. Deep-Sea Research A 33 (2), 225-246.

Ebersbach, F., Trull, T., Moy, C., 2006. Sinking Particle Properties Determined From Image Analysis of Polyacrylamide Gels Deployed in Drifting Sediment Traps During KEOPS: Implications for Ecosystem Controls on Carbon Export in the Presence of Persistent Natural Iron Inputs. Eos Trans. AGU, Ocean Sci. Meet. Suppl. 87 (36), Abstract OS35M-06.

Elskens, M., Baeyens, W., Boyd, P., Buesseler, K., Dehairs, F., Savoye, N., Van Mooy, B., 2008. Primary, new and export productions in the NW Pacific during the VERTIGO K2 experiments. Deep Sea Research II, this volume.

Eppley, R.W., 1989. New Production: History, Methods, Problems. In: Berger, W.H., Smetacek, V.S., Wefer, G. (Eds.), Productivity of the Ocean: Present and Past. Wiley, New York, pp. 85-97.

Fennel, K., Spitz, Y. H., Letelier, R. M., Abbott, M. R., and Karl, D. M. 2002. A deterministic model for N_2 fixation at stn. ALOHA in the subtropical North Pacific Ocean. Deep Sea Research II 49: 149-174.

Fowler, S.W., Knauer, G.A., 1986. Role of large particles in the transport of elements and organic compounds through the oceanic water column. Progress in Oceanography 16, 147-194.

Francois, R., Honjo, S., Krishfield, R., Manganini, S., 2002. Factors controlling the flux of organic carbon to the bathypelagic zone of the ocean. Global Biogechemical Cycles 16(4), 1087.

Holligan, P.M., Fernandez, E., Aiken, J., Balch, W.M., Boyd, P., Burkill, P.H., Finch, M., Groom, S.B., Malin, G., Muller, K., Purdie, D.A., Robinson, C., Trees, C.C., Turner,

S.M., Vanderwal, P., 1993. A Biogeochemical Study of the Coccolithophore, Emiliania-Huxleyi, in the North-Atlantic. Global Biogeochemical Cycles 7 (4), 879-900.

Honda, M.C., Imai, K., Nojiri, Y., Hoshi, F., Sugawara, T., Kusakabe, M., 2002. The biological pump in the northwestern North Pacific based on fluxes and major components of particulate matter obtained by sediment trap experiments (1997-2000). Deep-Sea Research I 49, 5595-5625.

Honda, M.C., Kawakama, H., Sasaoka, K., Watanabe, S., Dickey, T., 2006. Quick transport of primary produced organic carbon in the ocean interior. Geophysical Research Letters 33, L16603.

Honda, M.C., Watanabe, S., 2007. Utility of an automatic water sampler to observe seasonal variability in nutrients and DIC in the Northwestern North Pacific. Journal of Oceanography 63, 349-362.

Honjo, S., Manganini, S.J., 1993. Annual biogenic particle fluxes to the interior of the North Atlantic Ocean; studies at 34°N 21°W and 48°N 21°W. Deep-Sea Research II 40 (1-2), 587-607.

Hutchins, D.A., Bruland, K.W., 1998. Iron-limited diatom growth and Si:N uptake ratios in a coastal upwelling regime. Nature 393, 561-564.

Jiao, N.Z., Yang, Y.H., Koshikawa, H., Watanabe, M., 2002. Influence of hydrographic conditions on picoplankton distribution in the East China Sea. Aquatic Microbial Ecology 30 (1), 37–48.

Karl, D.M., Bidigare, R.R., Letelier, R.M., 2001. Long-term changes in plankton community structure and productivity in the subtropical North Pacific Ocean: The domain shift hypothesis. Deep-Sea Research II 48 (8-9), 1449-1470.

Karl, D.M., Bidigare, R.R., Letelier, R.M., 2002. Sustained and aperiodic variability in organic matter production and phototrophic microbial community structure in the North Pacific Subtropical Gyre. In: Willaims, P.J., Thomas, D.N., Reynolds, C.S. (Eds.), Phytoplankton Productivity. Blackwell Science Ltd, Oxford, pp. 222-264.

Karl, D.M., Christian, J.R., Dore, J.E., Hebel, D.V., Letelier, R.M., Tupas, L.M., Winn, C.D., 1996. Seasonal and interannual variability in primary production and particle flux at Station ALOHA. Deep-Sea Research II 43 (2-3), 539-568.

Karl, D.M., Lukas, R., 1996. The Hawaii Ocean Time-series (HOT) Program: Background, rationale and field implementation. Deep-Sea Research II 43 (2-3), 129-156.

Klaas, C., Archer, D.E., 2002. Association of sinking organic matter with various types of mineral ballast in the deep sea: Implications for the rain ratio. Global Biogechemical Cycles 16 (4), 1116, doi:1110.1029/2001GB001765.

Kobari, T., Steinberg, D.K., Ueda, A., Tsuda, A., Silver, M.W., Kitamura, M., 2008. Impacts of ontogenetically migrating copepods on downward carbon flux in the western subarctic Pacific Ocean. Deep Sea Research II, this volume.

Lam, P.J., Bishop, J.K.B., 2007. Is Dust Iron Supply to the Open Ocean Overblown? GRL, submitted.

Lamborg, C.H., Buesseler, K.O., Valdes, J., Bertrand, C.H., Bidigare, R., Manganini, S., Pike, S., Steinberg, D., Trull, T., Wilson, S., 2008. The Flux of Bio- and Lithogenic Material Associated with Sinking Particles in the Mesopelagic "Twilight Zone" of the Northwest and North Central Pacific Ocean. Deep Sea Research II, this volume-a.

Lamborg, C.H., Buesseler, K.O., Lam, P.J., 2008. Sinking fluxes of minor and trace elementes in the North Pacific Ocean measured during the VERTIGO program. Deep Sea Research II, this volume-b.

Lee, C., Murray, D.W., Barber, R.T., Buesseler, K.O., Dymond, J., Hedges, J.I., Honjo, S., Manganini, S., Marra, J., Moser, C., Peterson, M.L., Prell, W.L., Wakeham, S.G., 1998. Particulate organic carbon fluxes: Results from the U.S. JGOFS Arabian Sea Process Study. Deep-Sea Research II 45(10-11), 2489-2501.

Letelier, R.M., Dore, J.E., Winn, C.D., Karl, D.M., 1996. Seasonal and interannual variations in photosynthetic carbon assimilation at Station ALOHA. . Deep Sea Research II 43 (2-3), 467-490.

Letelier, R. M., Bidigare, R. R. Hebel, D. V. Ondrusek, M. Winn, C. K. and Karl, D. M. 1993. Temporal variability of the phytoplankton community structure based on pigment analyses. Limnology and Oceanography 38: 1420-1437.

Lipschultz, F., 2001. A time series assessment of the nitrogen cycle at BATS. Deep Sea Research II 48 (8-9), 1897-1924.

Liu, H., Suzuki, K., Saito, H., 2004. Community Structure and Dynamics of Phytoplankton in the Western Subarctic Pacific Ocean: A Synthesis Journal of Oceanography 60 (1), 119-137.

Lutz, M., Dunbar, R., Caldeira, K., 2002. Regional variability in the vertical flux of particulate organic carbon in the ocean interior. Global Biogeochemical Cycles 16 (3), 10.1029/2000GB001383.

Martin, J.H., Knauer, G.A., Karl, D.M., Broenkow, W.W., 1987. VERTEX: carbon cycling in the northeast Pacific. Deep-Sea Research A 34 (2), 267-285.

Michaels, A.F., Karl, D.M., Capone, D.G., 2001. Element stoichiometry, new production and nitrogen fixation. Oceanography 14(4), 68-77.

Michaels, A.F., Silver, M.W., 1988. Primary production, sinking fluxes and the microbial food web. Deep-Sea Research A 35(4), 473-490.

Nelson, D.M., Anderson, R.F., Barber, R.T., Brzezinski, M., Buesseler, K.O., Chase, Z., Collier, R.W., Dickson, M.-L., Francois, R., Hiscock, M., Honjo, S., Marra, J., Martin, W.R., Sambrotto, R.N., Sayles, F.L., Sigmon, D.E., 2002. Vertical budgets for organic carbon and biogenic silica in the Pacific sector of the Southern Ocean, 1996-1998. Deep-Sea Research II 49(9-10), 1,645-641,674.

Pike, S., Andrews, J., Trull, T., Buesseler, K., 2006. A high resolution study of particle export using Thorium-234 in the N. central Pacific and NW Pacific as part of the VERTIGO project. Ocean Sciences Meeting, Honolulu, HI.

Richardson, T.L., Jackson, G.A., 2007. Small Phytoplankton and Carbon Export from the Surface Ocean. Science 315, 838-840.

Richardson T. L., Cullen J. J., Kelley D. E., Lewis M. R., 1998. Potential contributions of vertically migrating Rhizosolenia to nutrient cycling and new production in the open ocean. Journal of Plankton Research **20**(2), 219-241.

Saito, M.A., Chisholm, S.W., Moffett, J.W., Waterbury, J., 2002. Cobalt limitation and uptake in the marine cyanobacterium *Prochlorococcus*. Limnology and Oceanography 47 (6), 1629-1636.

Sarthou, G., Timmermans, K.R., Blain, S., Treguer, P., 2005. Growth physiology and fate of diatoms in the ocean: a review. Journal of Sea Research 53 (1-2), 25-42.

Scholten, J.C., Fietzke, J., Vogler, S., Rutgers van der Loeff, M., Mangini, A., Koeve, W., Stoffers, P., Antia, A.N., Neuer, S., Waniek, J., 2001. Trapping efficiencies of sediment traps from the deep eastern North Atlantic: The 230Th calibration. Deep-Sea Research II 48(10), 2383-2578.

Sharek, R., Tupas, L.M., Karl, D.M., 1999. Diatom fluxes to the seep sea in the oligotrophic North Pacific gyre at Station ALOHA. Marine Ecology Progress Series 182, 55-67.

Siegel, D.A., Deuser, W.G., 1997. Trajectories of sinking particles in the Sargasso Sea: Modeling of statistical funnels above deep-ocean sediment traps. Deep-Sea Research I 44 (9-10), 1,519-1,541.

Siegel, D.A., Fields, E., Buesseler, K.O., 2007. A bottom-up view of the biological pump: Modeling source funnels above ocean sediment traps. Deep Sea Research I, in press.

Siegel, D.A., Granata, T.C., Michaels, A.F., Dickey, T.D., 1990. Mesoscale eddy diffusion, particle sinking, and the interpretation of sediment trap data. Journal of Geophysical Research 95 (C4), 5305-5311.

Steinberg, D.K., Cope, J.S., Wilson, S.E., Kobari, T., 2008. A comparison of mesopelagic zooplankton community structure in the subtropical and subarctic Pacific Ocean. Deep Sea Research II, this volume.

Steinberg, D.K., Van Mooy, B.A.S., Buesseler, K.O., Boyd, P.W., Kobari, T., Karl, D.M., 2007. Microbial vs. zooplankton control of sinking particle flux in the ocean's twilight zone. Limnology and Oceanography, in press.

Singler H. R., Villareal T. A., 2005. Nitrogen inputs into the euphotic zone by vertically migrating Rhizosolenia mats. Journal of Plankton Research **27**(6), 545-556.

Trull T. W., Bray S., Buesseler K. O., Lamborg C. H., Manganini S., Moy C., and Valdes J. , 2008. In-situ measurement of mesopelagic particle sinking rates and the control of carbon transfer to the ocean interio during the Vertical Flux in the Global Ocean (VERTIGO) voyages in the North Pacific. *Deep Sea Research II*, this volume.

Volk, T., Hoffert, M.I., 1985. Ocean carbon pumps: Analysis of relative strengths and efficiencies in ocean-drive atmospheric CO2 changes. Geophysical Monographs 32, 99-110.

Wefer, G., Fischer, G., 1991. Annual primary production and export flux in the Southern Ocean from sediment trap data. Marine Chemistry 35, 597-613.

Wilson, S.E., Steinberg, D.K., Buesseler, K.O., 2008. Changes in fecal pellet characteristics with depth as indicators of zooplankton repackaging of particles in the mesopelagic zone. Deep Sea Research II, this volume.

Yayanos, A.A., Benson, A.A., Nevenzel, J.C., 1978. The pressure-volume-temperature (PVT) properties of a lipid mixture from a marine copepod, Calanus plumchrus: implications for buoyancy and sound scattering. Deep-Sea Research 25 (3), 257-268.

Yu, E.-F., Francois, R., Bacon, M.P., Honjo, S., Fleer, A.P., Manganini, S.J., Rutgers van der Loeff, M.M., Ittekot, V., 2001. Trapping efficiency of bottom-tethered sediment traps estimated from the intercepted fluxes of ^{230}Th and ^{231}Pa. Deep-Sea Research I 48 (3), 865-889.

Zhang, Y., Jiao, N.Z., Hong, N., 2008. Comparative studies on picoplankton biomass and community structure in different provinces from subarctic to subtropical oceans. Deep Sea Research II, this volume.

Figure 1.

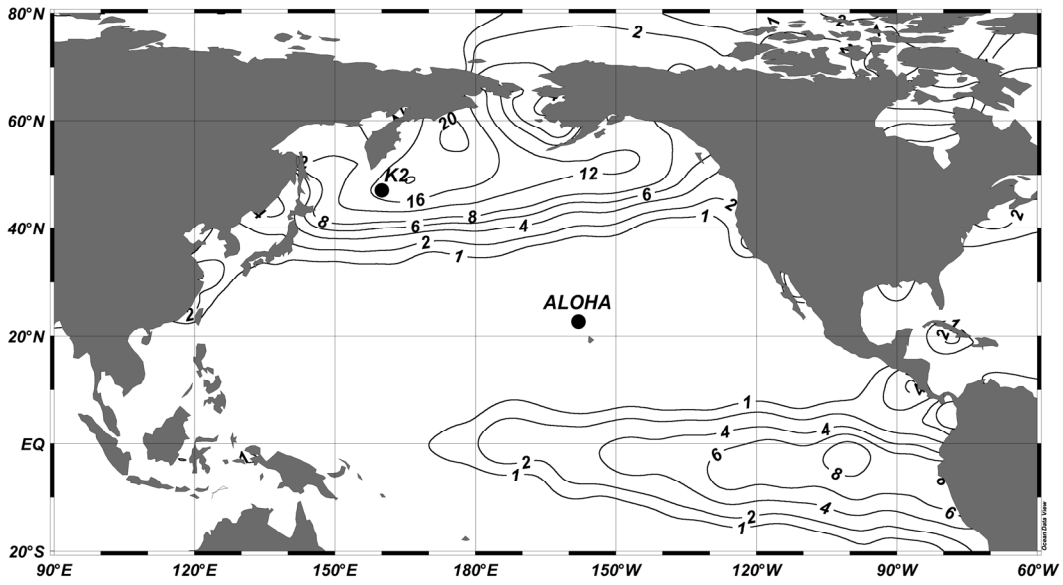
80°N
60°N
40°N
20°N
EQ
20°S
90°E
120°E
150°E
180°E
150°W
120°W
90°W
60°W
K2
ALOHA
2
20
12
16
6
8
4
1
Ocean Data View

Figure 2.

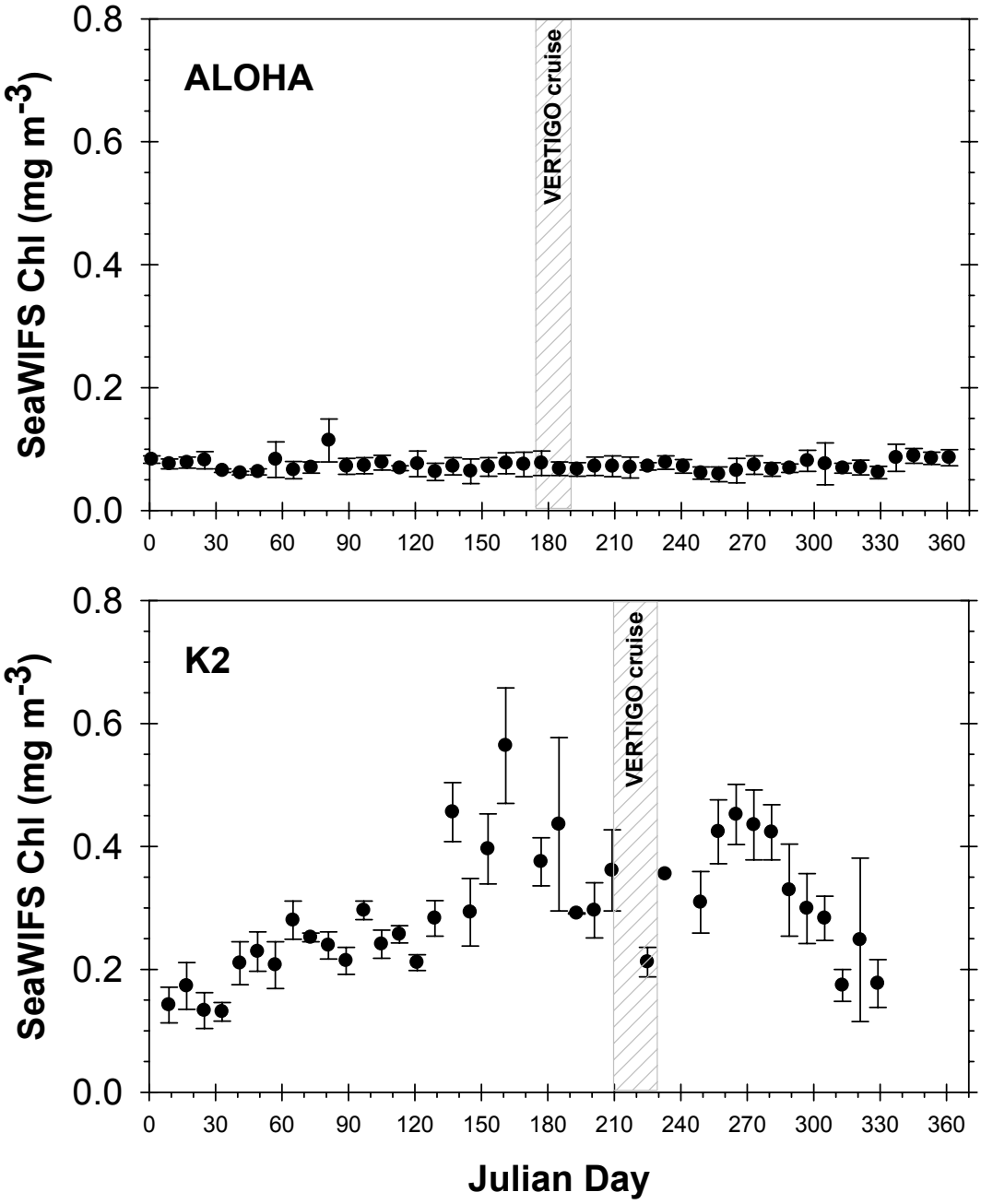
ALOHA
VERTIGO cruise
SeaWIFS Chl (mg m-3)
0.0
0.2
0.4
0.6
0.8
0
30
60
90
120
150
180
210
240
270
300
330
360
K2
VERTIGO cruise
SeaWIFS Chl (mg m-3)
Julian Day

Figure 3.

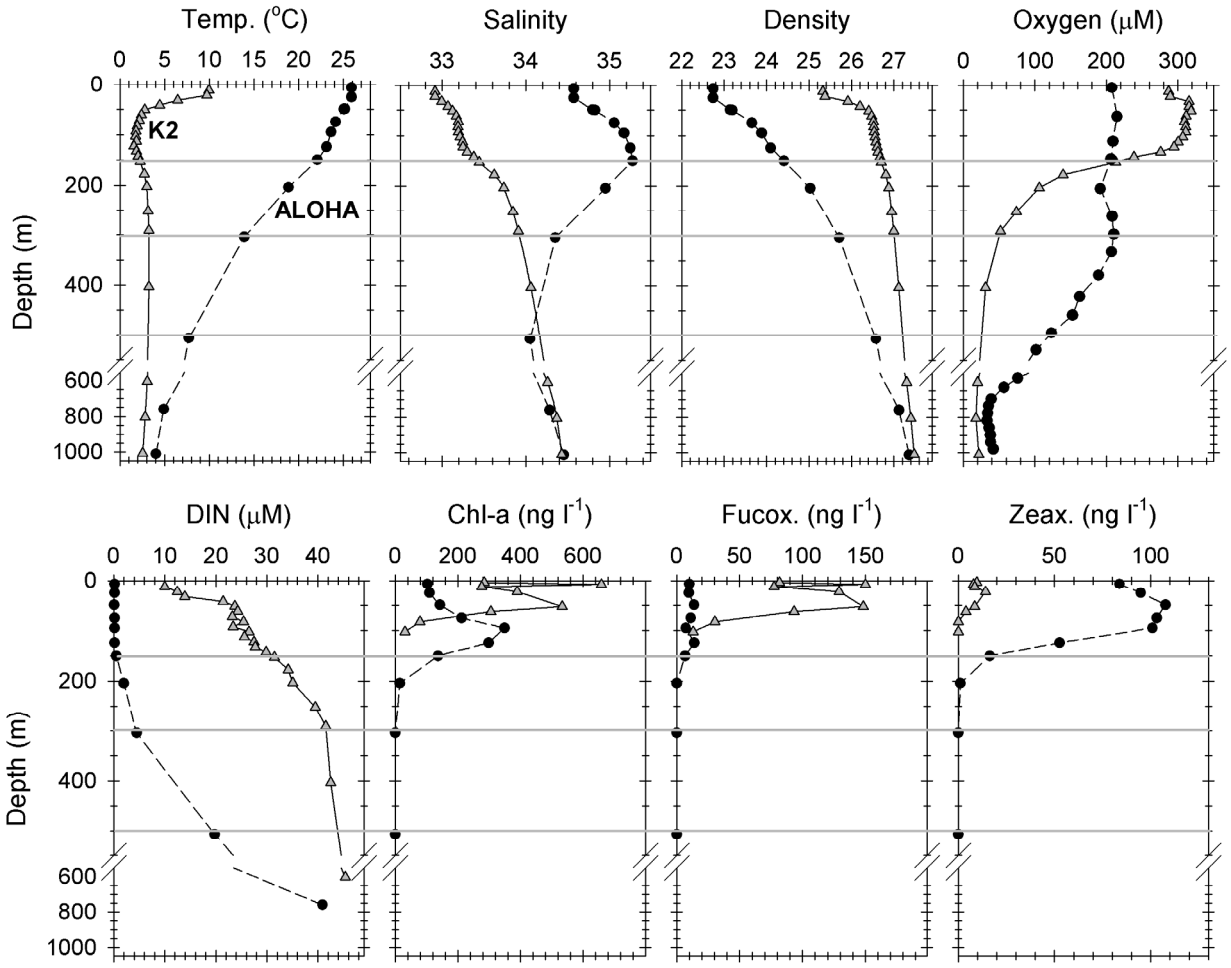
Temp. (°C)
Salinity
Density
Oxygen (μM)
K2
ALOHA
Depth (m)
DIN (μM)
Chl-a (ng l-1)
Fucox. (ng l-1)
Zeax. (ng l-1)

Figure 4.

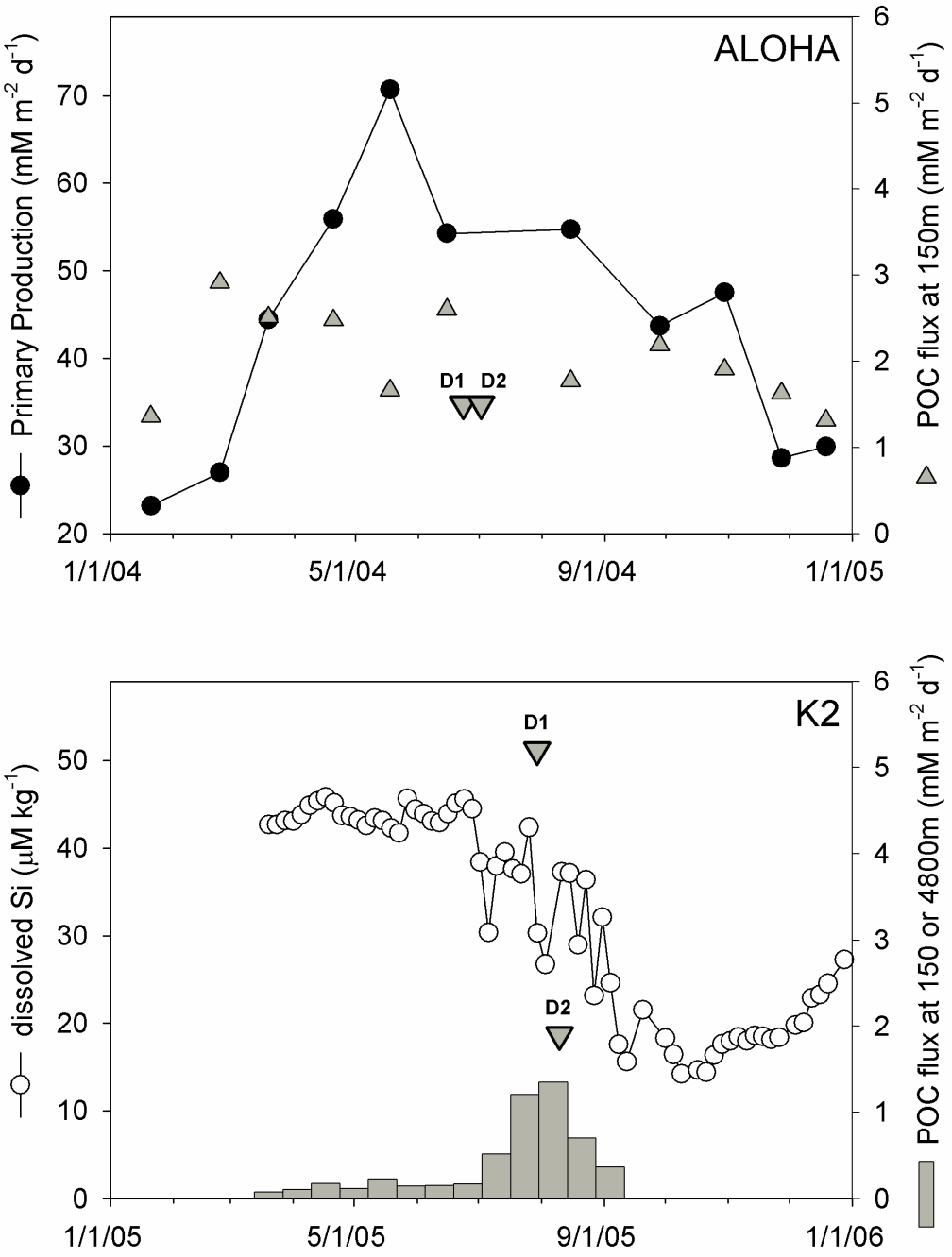
ALOHA
Primary Production (mM m-2 d-1)
POC flux at 150m (mM m-2 d-1)
D1
D2
1/1/04
5/1/04
9/1/04
1/1/05
K2
dissolved Si (µM kg-1)
POC flux at 150 or 4800m (mM m-2 d-1)
1/1/05
5/1/05
9/1/05
1/1/06

Figure 5.

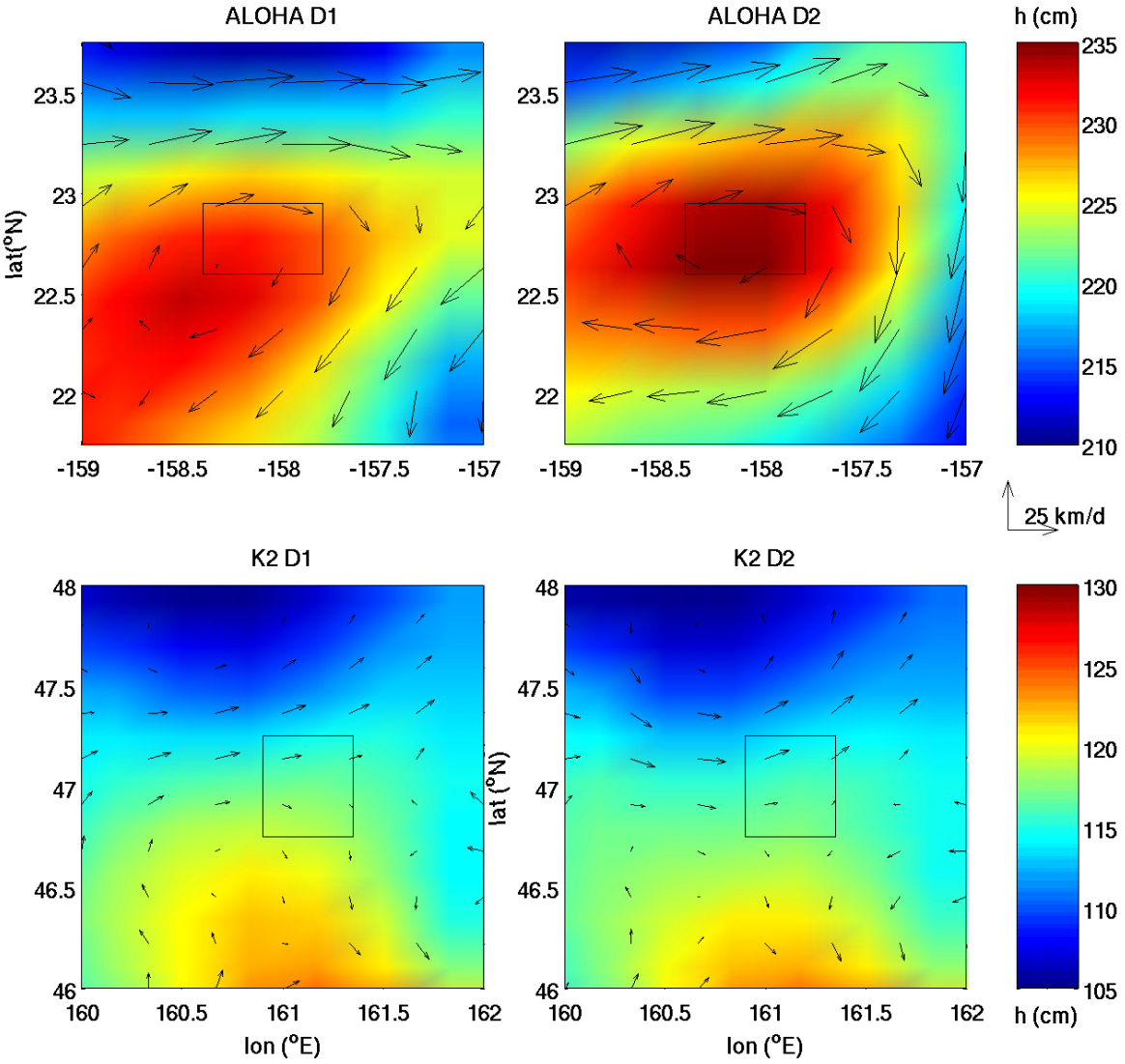
ALOHA D1
ALOHA D2
h (cm)
235
230
225
220
215
210
23.5
23
22.5
22
lat(°N)
-159
-158.5
-158
-157.5
-157
25 km/d
K2 D1
K2 D2
48
47.5
47
46.5
46
lat (°N)
160
160.5
161
161.5
162
lon (°E)
130
125
120
115
110
105
h (cm)

Figure 6.

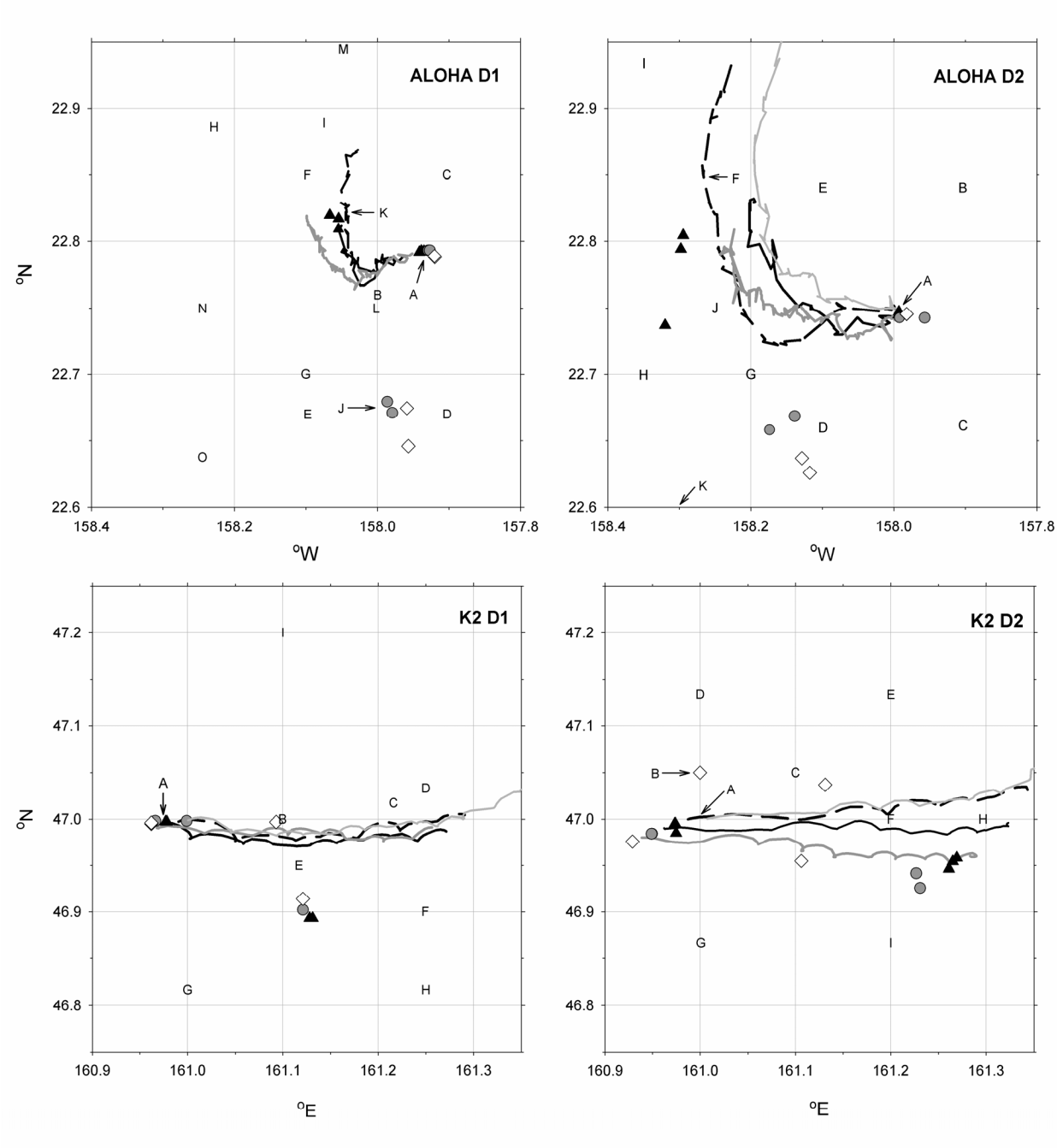
ALOHA D1
ALOHA D2
K2 D1
K2 D2
°N
°W
°E
22.9
22.8
22.7
22.6
158.4
158.2
158.0
157.8
47.2
47.1
47.0
46.9
46.8
160.9
161.0
161.1
161.2
161.3

Figure 7.

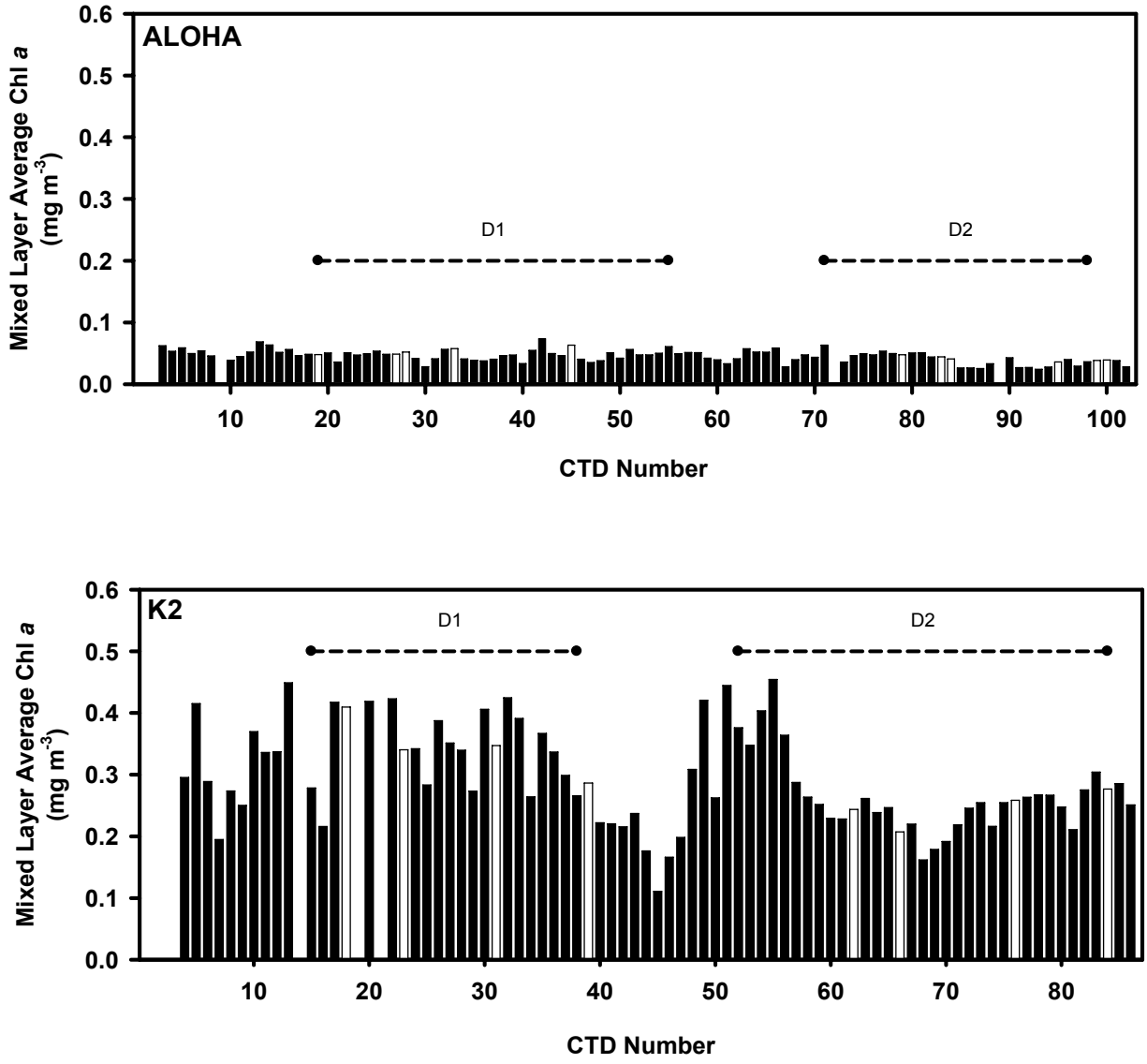
ALOHA
Mixed Layer Average Chl a (mg m-3)
0.6
0.5
0.4
0.3
0.2
0.1
0.0
D1
D2
10
20
30
40
50
60
70
80
90
100
CTD Number
K2
Mixed Layer Average Chl a (mg m-3)
0.6
0.5
0.4
0.3
0.2
0.1
0.0
D1
D2
10
20
30
40
50
60
70
80
CTD Number

Figure 8.

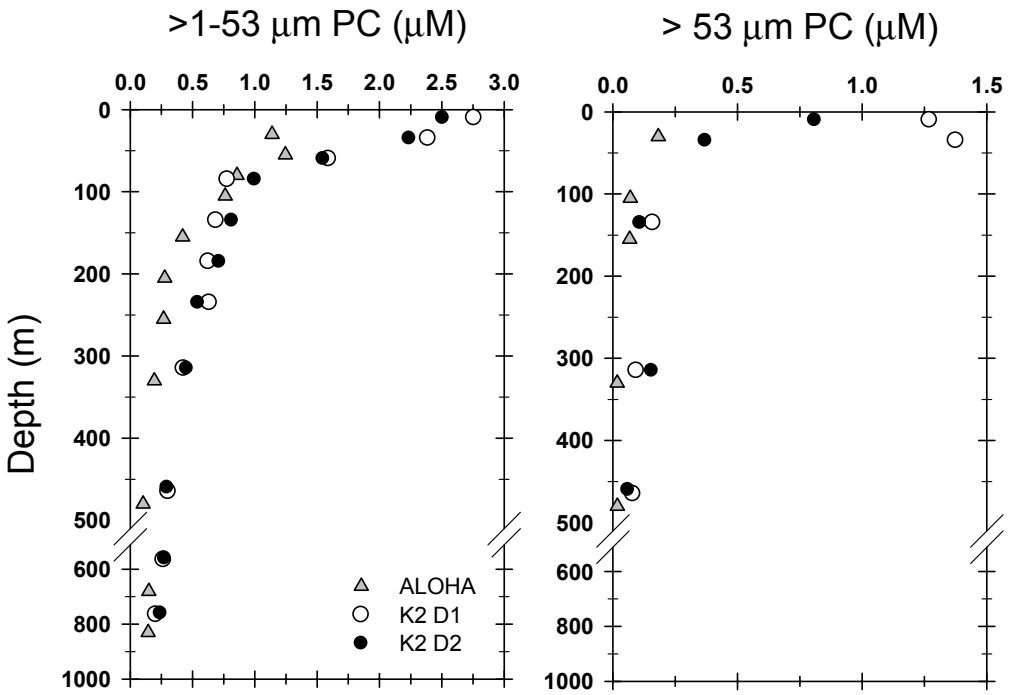
>1-53 μm PC (μM)
> 53 μm PC (μM)
Depth (m)
0.0
0.5
1.0
1.5
2.0
2.5
3.0
0
100
200
300
400
500
600
800
1000
ALOHA
K2 D1
K2 D2

Figure 9.

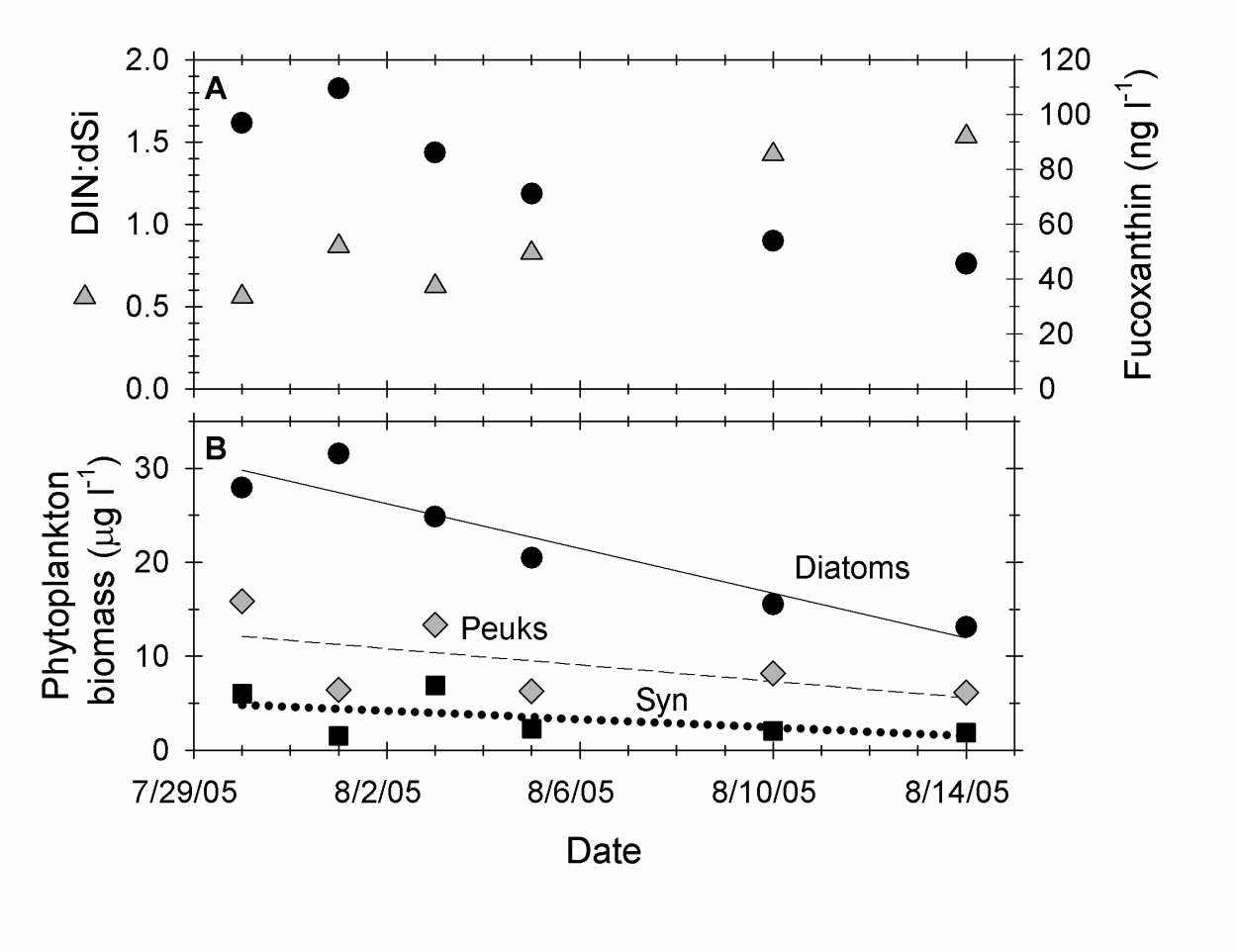
A
B
DIN:dSi
Fucoxanthin (ng l-1)
Phytoplankton biomass (µg l-1)
Diatoms
Peuks
Syn
7/29/05
8/2/05
8/6/05
8/10/05
8/14/05
Date

Figure 10.

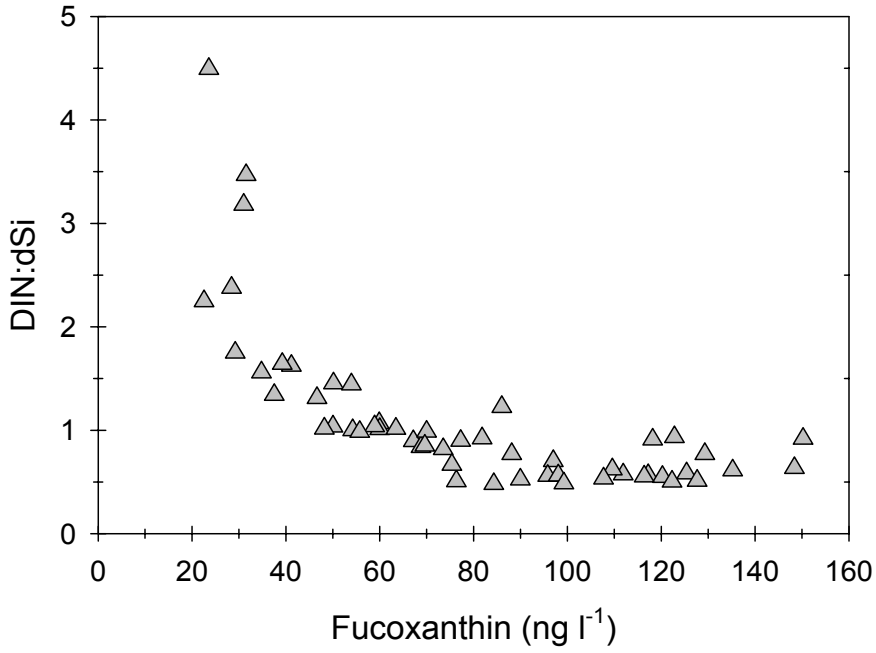

Figure 11.

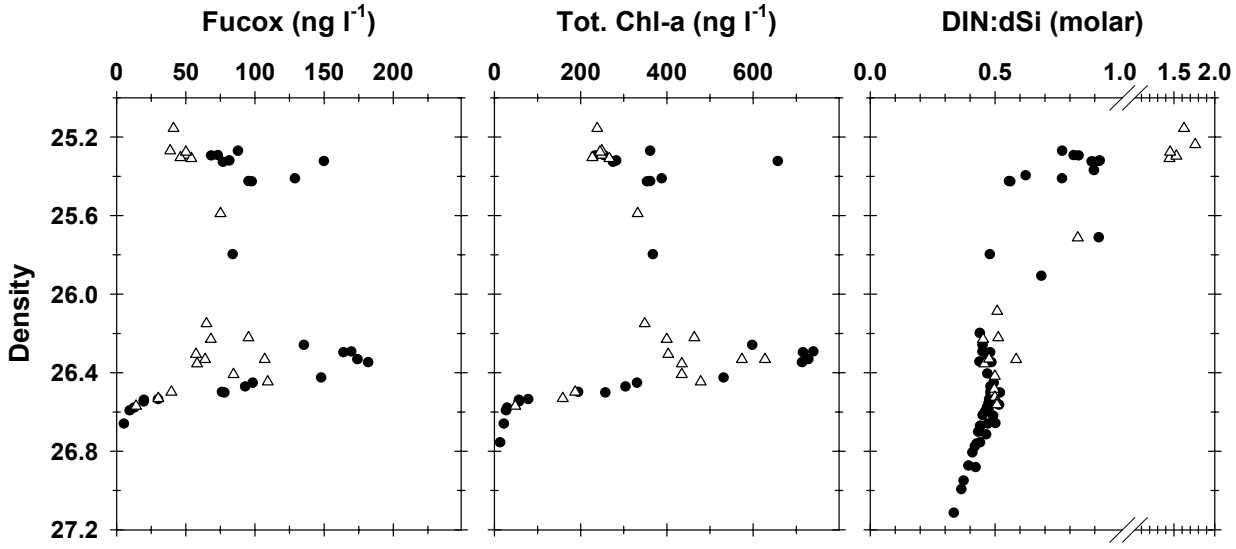
Fucox (ng l-1)
Tot. Chl-a (ng l-1)
DIN:dSi (molar)
Density
0
50
100
150
200
0
200
400
600
0.0
0.5
1.0
1.5
2.0
25.2
25.6
26.0
26.4
26.8
27.2

Figure 12.

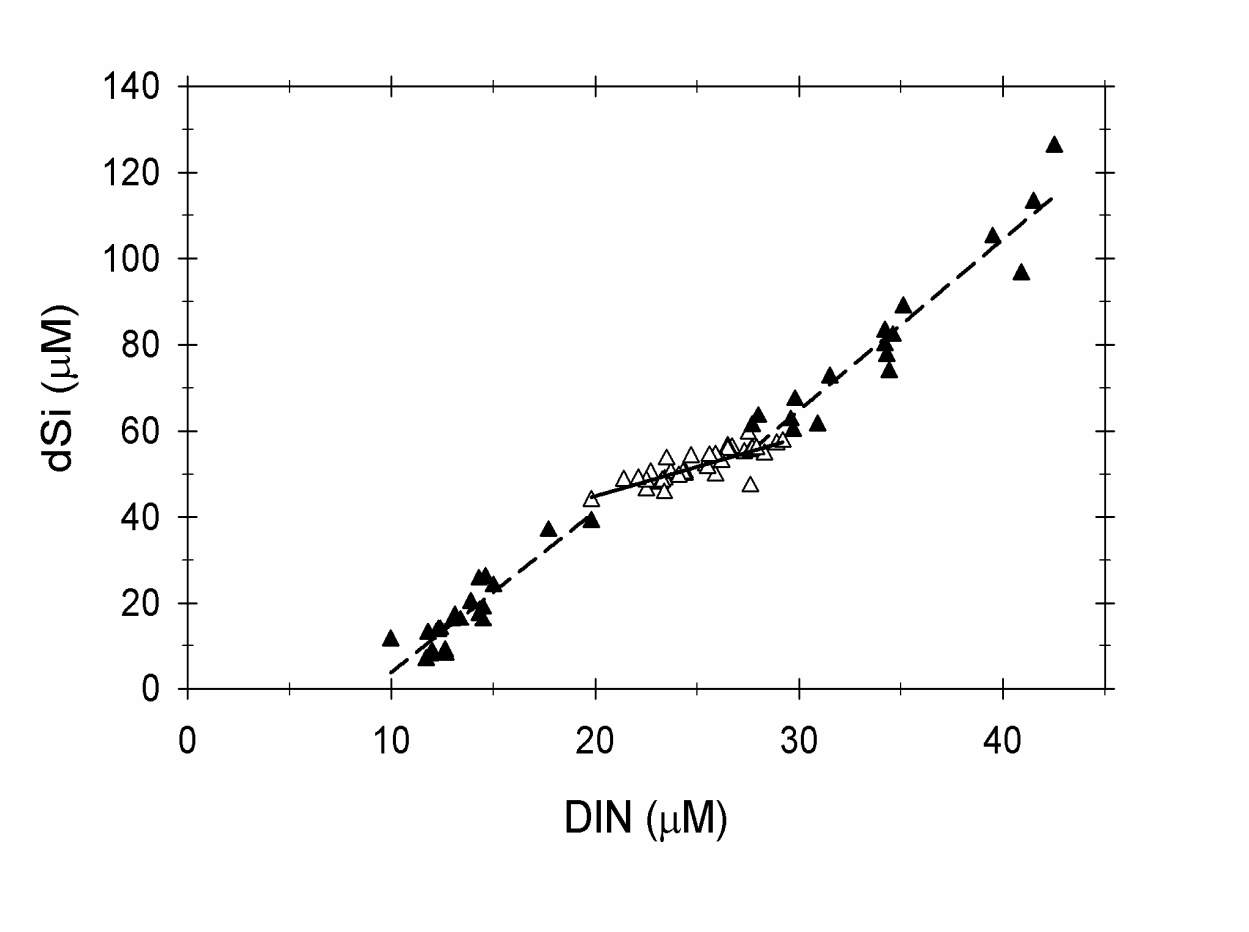

Figure 13.

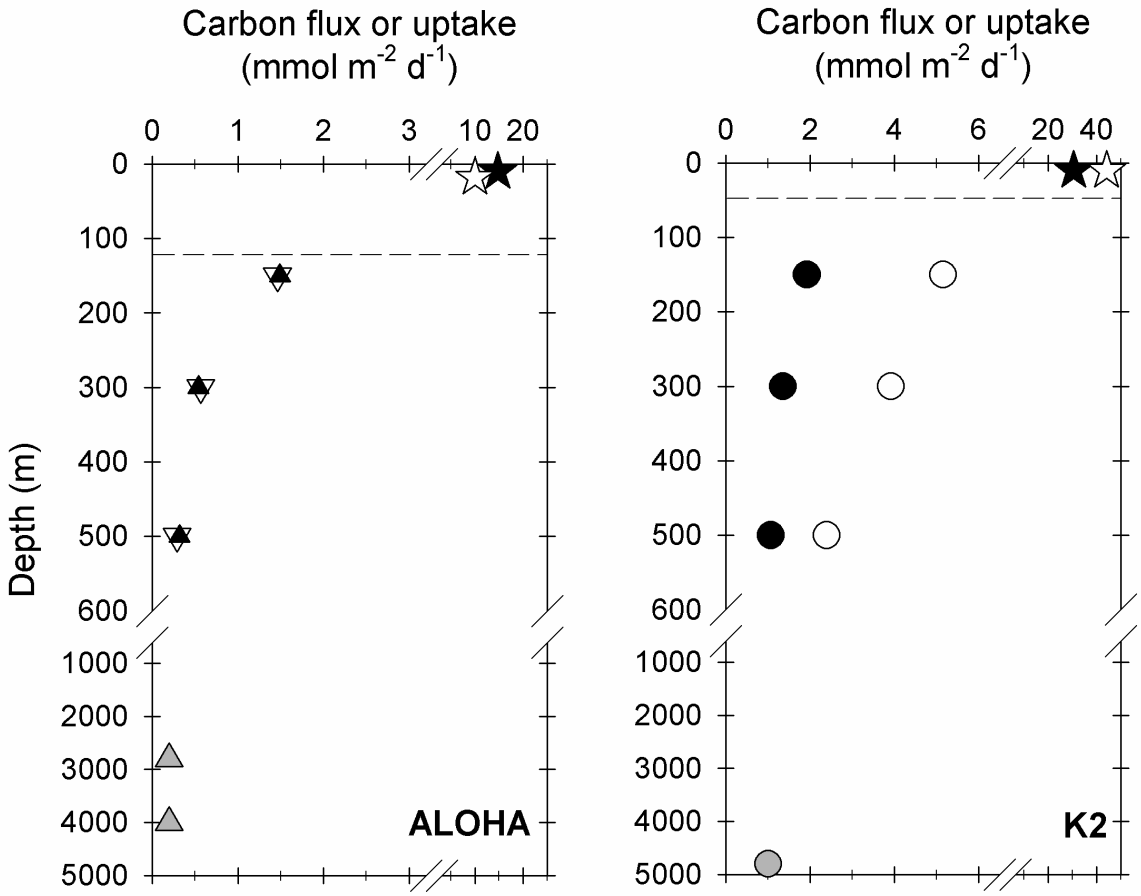
Carbon flux or uptake
(mmol m-2 d-1)
0 1 2 3 10 20
Depth (m)
0 100 200 300 400 500 600 1000 2000 3000 4000 5000
ALOHA
Carbon flux or uptake
(mmol m-2 d-1)
0 2 4 6 20 40
0 100 200 300 400 500 600 1000 2000 3000 4000 5000
K2

Figure 14.

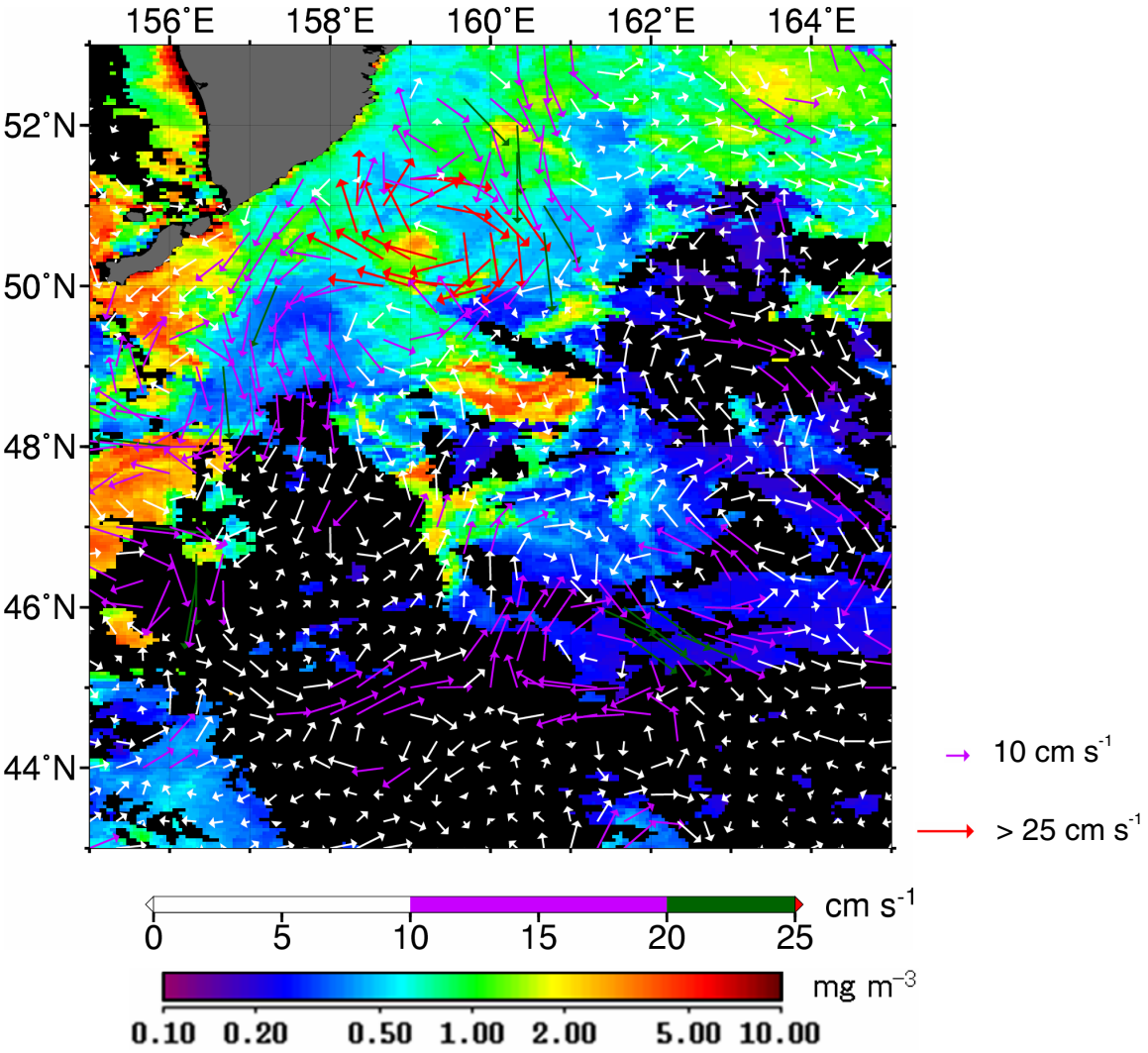
156˚E
158˚E
160˚E
162˚E
164˚E
52˚N
50˚N
48˚N
46˚N
44˚N
10 cm s-1
> 25 cm s-1
cm s-1
0
5
10
15
20
25
mg m-3
0.10
0.20
0.50
1.00
2.00
5.00
10.00